ELSEVIER

International Journal of Mass Spectrometry 214 (2002) 175–212

International Journal of Mass Spectrometry

www.elsevier.com/locate/ijms

Review

The binding energies of small Ar, CO and N_2 cluster ions

Karl-Michael Weitzel*, Joachim Mähnert

Institut für Chemie, Physikalische und Theoretische Chemie, Freie Universität Berlin, Takustr. 3, 14195 Berlin, Germany

Received 16 July 2001; accepted 18 December 2001

Abstract

This article reviews the available information on the thermochemistry of argon, carbon monoxide and nitrogen cluster ions with focus on kinetic energy release (KER) studies of the dissociative ionization of neutral clusters performed in the authors laboratory. The latter constitutes a variant of translational energy spectroscopy (TES). The information derived includes the adiabatic ionization energies and the binding energy of small cluster ions. Here we present experimental data together with extensive theoretical calculations of the KER based on ab initio structure data. The theories employed range from simple empirical formula which allow a quick estimate of the KER to extensive phase space theory calculations. The binding energies of the ions are: $D_0(Ar_2^+) = 1.29\,eV$, $D_0(ArN_2^+) = 1.19\,eV$, $D_0(ArCO^+) = 1.00\,eV$, and $D_0((N_2)_2^+) = 1.06\,eV$. The binding energy of the $C_2O_2^+$ is $D_0(C_2O_2^+) = 1.80\,eV$, significantly larger than many previous values. The latter represents in fact a molecular ion. (Int J Mass Spectrom 214 (2002) 175–212)

Keywords: Cluster; Ionization energy; Binding energy; Dissociation ionization; Kinetic energy release

1. Introduction

A general classification of clusters according to their binding strength into van der Waals clusters, molecular clusters, hydrogen bonded clusters, ionic clusters, valence clusters and metal clusters has been proposed by Jortner [1]. The current review focuses on small aggregates, which are bound by weak van der Waals forces in the neutral state. Here, we consider the dimers with one van der Waals bond as the smallest cluster entities. One of the current questions in cluster science is whether intermolecular and intramolecular vibrational modes equally participate in the energy flow in the cluster. Examples of both, mode selective dissociation in small HCN clusters [2,3] and statistical decay of ethylchloride clusters with participation of all vibrational modes [4] can be found in the literature. However, no simple border lines between these limiting cases are available today. In this context the variation of chemical reactivity with increasing solvation receives significant interest [5,6]. Surprisingly, for some of the most fundamental properties of small clusters, the ionization energy (IE) and the ionic binding energies, literature data differ in some cases by more than 1 eV.

The majority of thermochemical data [7] available for cluster ions today [8,9] is coming from high pressure mass spectrometry [10] and from studies of ion/molecule reactions, e.g., by means of selected ion flow drift tube (SIFDT) experiments [11]. While these experiments and corresponding theoretical analysis [12] focus on the heat of reaction and kinetic

* Correspondig author. E-mail: weitzel@chemie.fu-berlin.de

1387-3806/02/$20.00
PII S1387-3806(02)00522-5

information, very accurate spectroscopic and structural information on weakly bound cluster ions has been derived from infrared photodissociation (IRPD) studies [13]. The most important source for ionization energies of cluster has been the photoionization of neutral cluster beams [14]. However, there is one fundamental problem. Due to the fact that neutral cluster beams are in general characterized by some distribution of cluster sizes, the origin of a cluster ion observed in a mass spectrometer is not unambiguous. This cluster ion may either be formed by ionization of the corresponding neutral cluster or by ionization of a larger cluster followed by spontaneous dissociation of the primary cluster ion. The latter is generally referred to as dissociative ionization. In order to derive accurate IEs it is important to identify the dissociative ionization and take it into account in the analysis. It is the aim of this work to review a simple technique which allows to identify the dissociative ionization of clusters by means of measuring the kinetic energy released in this process. This constitutes a variant of translational energy spectroscopy (TES). Ultimately this technique provides access to improved ionization energies and ionic binding energies. The advantages and limitations of this technique will be discussed.

2. Theoretical aspects

2.1. Energy selection of ions

One of the primary tasks in studying chemical reactions of ions is the characterization of the reacting ensemble. In general two different concepts are employed in ion chemistry. The first is lifetime selection which is, e.g., the standard approach in mass analyzed ion kinetic energy spectroscopy (MIKES) [15]. The second is energy selection often employed when looking at the energetics and kinetics of ionic reactions. The latter technique is also employed in this work. The experiments covered by this review deal with the reactions of cluster ions formed by photoionization from neutral precursors. Since an electron is ejected in the photoionization step, the internal energy of the ion, E_{int}, whose chemical reaction is subsequently investigated is given by Eq. (1)

$$E_{\mathrm{int}} = h\nu + E_{\mathrm{th}} - \mathrm{IE} - E_{\mathrm{el}} \quad (1)$$

where $h\nu$ is the photon energy, IE the adiabatic ionization energy of the molecule, E_{th} the thermal energy of the sample and E_{el} the kinetic energy of the electron ejected. According to Eq. (1) the internal energy of the ion is only known if the kinetic energy of the corresponding electron is also known. This is the basis of the photoelectron–photoion coincidence technique (PEPICO) [16,17]. Various different coincidence techniques are available to study singly charged ions, energetic PEPICO [18], threshold PEPICO (TPEPICO) [16,17], and pulsed field ionization PEPICO (PFI-PEPICO) [19].

2.2. Release of kinetic energy in a dissociative ionization

Much of the current knowledge on the structure and ionization energy of clusters is due to photoionization (PI) and electron impact (EI) ionization of cluster beams [20–22]. However, since cluster beams are in general characterized by a distribution of different cluster sizes the assignment of a given cluster ion signal to a specific neutral precursor is not unambiguous. Consider a beam consisting of homogeneous clusters $(\mathrm{AB})_m$ with $m > 1$, than there is more than one way to form a cluster ion $(\mathrm{AB})_n{}^+$, with $n < m$. First the ion $(\mathrm{AB})_n{}^+$ can be formed by non-dissociative ionization from a neutral cluster $(\mathrm{AB})_n$ as indicated in Eq. (2).

$$(\mathrm{AB})_n + h\nu \rightarrow (\mathrm{AB})_n{}^+ + \mathrm{e}^- \quad (2)$$

The ion $(\mathrm{AB})_n{}^+$ can also be formed via the ionization of a larger cluster with consecutive fragmentation. This path indicated in Eq. (3) is termed dissociative ionization.

$$\begin{aligned}(\mathrm{AB})_{n+1} + h\nu &\rightarrow (\mathrm{AB})_{n+1}{}^+ + \mathrm{e}^- \\ &\rightarrow (\mathrm{AB})_n{}^+ + (\mathrm{AB}) + \mathrm{e}^- \end{aligned} \quad (3)$$

If this fragmentation is fast on the time scale of the experiment both pathways will lead to the observation of an ion $(\mathrm{AB})_n{}^+$ in a mass spectrometer

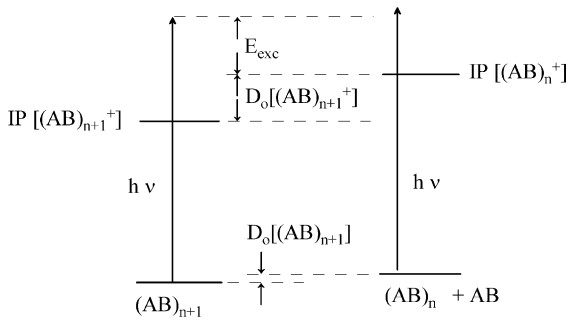

Fig. 1. Balance of energy in the dissociative ionization of clusters.

and will thus cause problems with the assignment. Here it is important to discuss the energy balance for the different ionization pathways as illustrated in Fig. 1.

If the ion $(AB)_n^+$ is formed via non-dissociative ionization (Eq. (2)), its internal energy is given by Eq. (1) and the translational energy will be the translational energy of the cluster beam, i.e., very small. If, on the other hand the $(AB)_n^+$ ions are formed by dissociative ionization of an $(AB)_{n+1}$ cluster (Eq. (3)) the excess energy of the intermediate $(AB)_{n+1}^+$ ion will be distributed over the degrees of freedom of the products (translation, vibration, rotation) in the dissociation event as indicated in Eq. (4)

$$E_{\text{exc}} = E_{\text{v}}[(AB)_n^+ + AB] + E_{\text{rot}}[(AB)_n^+ + AB] + E_{\text{trans}}[(AB)_n^+ + AB] \quad (4)$$

The last term in Eq. (4) is the total kinetic energy released into the products in the reaction (throughout this work the discussion of KER refers to the center of mass of the cluster). In general the translational energy of a dissociatively formed ion $(AB)_n^+$ will be larger than that of an $(AB)_n^+$ formed by non-dissociative ionization. The vibrational energy, on the other hand, is often lower in the dissociative case. This is the basis of the evaporative cooling of clusters [23], where clusters stabilize by boiling off parts—preferentially monomer units. The 70 eV EI of a large cluster can lead to a chain of consecutive fragmentation steps along which the internal energy keeps decreasing until the fragmentation ultimately stops. Finally we note that the rotational energy of dissociatively formed cluster ions may well be significantly larger than that of the initial neutral cluster beam and may influence the rate constant. This is most likely the reason for the metastable decay of Ar_3^+ ions which was explained by tunneling of Ar atoms through a centrifugal barrier [24,25]. We believe that the very high rotational quantum numbers inferred ($J \approx 60$) are the result of the dissociative ionization of larger clusters. This discussion shows that in general the mass is the only property which ions $(AB)_n^+$ formed by the two pathways (Eqs. (2) and (3)) have in common. They differ in all other properties like internal or translational energy. Consequently, important cluster properties depending on the latter, e.g., chemical reactivity, will be influenced by the presence of dissociative ionization. This also holds true for the determination of ionization energies.

The dissociative ionization already discussed is particularly important in cases where a cluster cannot be ionized efficiently at its adiabatic IE due to significant differences in the equilibrium geometry of the neutral and the ion, which leads to vanishing Franck–Condon factors for one photoionization. This is in fact the case for most small van der Waals clusters, e.g., for the argon trimer, the neutral ground state is triangular [26] while the ion ground state is linear [27]. Ionization is in this case only possible at significantly higher excitation energies. In many cases the vertical transition in the accessible Franck–Condon region even leads to energies which lay above the dissociation threshold. Just measuring the appearance energy of some cluster ion will in this case only yield an upper bound to the IE. In the past one often tried to diminish this problem by investigating the AE of a small cluster ion under very mild expansion conditions, where no large clusters are expected to be formed in the neutral cluster beam [14].

This review discusses the implementation of an alternative technique which allows to distinguish dissociative from non-dissociative ionization and ultimately lead to a new approach for determining the IEs of small clusters. In principle any of the energy components discussed can be used for this distinction. Here, we

choose the kinetic energy of cluster ions as an indicator of the dissociative ionization. For isolated molecular ions the measurement of the KER in a unimolecular reaction has a long standing tradition [28]. For a cluster system the release of kinetic energy in a dissociative photoionization was to our knowledge first observed by Ding and coworkers [29]. Later such KER has also been observed by Weitzel et al. [4], Baer and coworkers [30,31], and Furuya and Kimura [32]. However, in none of these studies IEs or binding energies have been derived from the KER (note, [4] reports the IE of ethylchloride dimers, but that was derived from a rate constant analysis). The determination of thermochemical threshold energies should in principle be possible by comparison of experimental KER data with theoretical estimates in an experiment combining EI of a cluster with MIKES analysis [33]. This is based on the fact that in general any simple bond fission will be accompanied by a finite KER. For a simple bond fission, the KER is expected to approach zero right at the thermochemical threshold of the process, i.e., the KER is characteristic for the threshold energy. [1] This concept was, e.g., employed in the determination of the binding energy of protonated ammonia clusters [34] by measuring the KER in the metastable decay of mass-selected clusters. In that experiment the internal energy of the cluster ions is not well established and certainly difficult to vary in a controlled way. Evidently measuring the KER as a function of the internal energy of cluster ions would provide more accurate access to threshold energies. This is the explicit goal of the current work. Here, parent cluster ions with well defined internal energy are formed by photoionization with subsequent energy selection of the ions. Systematic KER measurements are presented as a function of the ion internal energy. This experimental KER is extrapolated to zero KER either directly or by comparison with theoretical KER curves, which in turn allows the determination of threshold energies.

[1] Concerted elimination reactions, on the other hand, often have non-zero KER at the threshold.

2.3. Determination of the KER from time-of-flight spectra

Let us assume we prepare a microcanonical ensemble of molecules with an excess energy $E_{\mathrm{exc}} > 0$ above its dissociation threshold. Then this excess energy will be distributed over the degrees of freedom of the products (translation, rotation, vibration) formed in the reaction. Thus, in general any unimolecular reaction will be accompanied by a finite KER. The KER is an important quantity in the characterization of elementary reactions. The measurement of KER distributions (KERDs) is, e.g., the basis of the photofragment spectroscopy [35,36]. In recent years a modification of this, the H atom translational spectroscopy by Rydberg tagging [37,38] has received considerable interest. The KER experiments covered by this review also belong into the field of translational energy spectroscopy. The analysis of KERD is important for determining reaction mechanisms. The maximum of the KERD peaks at KER $= 0$ in the case of a simple bond fission in a statistical reaction [39]. The maximum of the KERD will, however, occur for KER > 0 in the case of a reaction with a high barrier for the reverse reaction.

For a discussion of the energy balance according to Eq. (4) it is often sufficient to study the average kinetic energy of the relevant cluster ions. This kinetic energy can be either due to the translational temperature of the precursor clusters and/or to the KER in a photo-induced dissociation. The measurement of the average kinetic (translational) energy of ions is easily possible in a time-of-flight mass spectrometer (TOF-MS). Experimental aspects will be discussed separately in a later section. Here we concentrate on the methodological concept. In a linear TOF-MS any distribution of translational energy of ions formed in the ion source will lead to a distribution of arrival times. The width of this distribution correlates with the turn around time of ions with an initial velocity vector pointing away from the detector. By using small electric fields we can ensure that the full-width at half-maximum (FWHM) of the ion signal in the TOF domain is dominated by the kinetic energy of the ions formed in the ion source. For molecular ions

of mass M_P formed in the ion source the average kinetic energy (KE) of the ions in the molecular frame is related to the FWHM of the ion signal in the TOF domain (laboratory frame) by Eq. (5) [40]:

$$\mathrm{KE} = \frac{3(qE\mathrm{FWHM_t})^2}{16 \ln 2 M_P} \quad (5)$$

where E is the electric field in the ion source, q the charge of the molecular ion (in this work always: $q = +1$). Eq. (5) holds strictly only for the case of a thermal velocity distribution [41,42] characterized by a temperature T (KE = 3/2 kT). The validity of Eq. (5) has been verified for various ions and electric fields [43]. If the ion has been formed by a dissociative process the kinetic energy consists of contributions from the KER and from the conservation of the linear momentum of the parent cluster. In this case the total average kinetic energy released in the dissociation is given by [40]:

$$\mathrm{KER} = \frac{3M_P(qE\,\mathrm{FWHM_t})^2}{16 \ln 2 M_N M_D} - \frac{M_D \mathrm{KE_P}}{M_N} \quad (6)$$

where M_P, M_D and M_N are the mass of the parent and the fragment ion and the neutral fragment. $\mathrm{FWHM_t}$ is the full-width half-maximum of the fragment ion in the TOF domain. $\mathrm{KE_P}$ is the kinetic energy of the parent ion at the time of its formation (Eq. (5)). The average total KER is in general dominated by the first term in Eq. (6). The second term stems from the conservation of the linear momentum of the parent ion. This total KER is distributed over all fragments. That part of the total KER, which shows up in the fragment ion (D^+) is obtained from the total KER by multiplication with M_N/M_P.

$$\mathrm{KER}(D^+) = \frac{3(qE\mathrm{FWHM_t})^2}{16 \ln 2 M_D} - \frac{M_D \mathrm{KE_P}}{M_P} \quad (7)$$

All experiments of this work have been performed in cold cluster beams, where the second term is typically on the order of few meV and thus negligible. Throughout this work the term KER will be used synonymously with the total average KER. That part of the KER associated with the fragment ion will be denoted KER(D^+). Eqs. (6) and (7) strictly hold only in the case of thermal isotropic KER distribution. The validity of making such an assumption is experimentally supported by the fact that all TOF distributions discussed in this work have Gaussian shape. Deviations from this could, e.g., be caused by a mono-energetic KER leading to a rectangular TOF distribution [42]. This is expected for non-statistical reactions from a repulsive potential surface [44] or in the case of a significant barrier for the reverse reaction [45].

In the past the measurement of the KER in dissociative ionization has provided valuable information on numerous elementary reactions. Again, we mention the two major different techniques, (i) the investigation of the KER in the fragmentation of energy-selected ions [28]—in general as a function of the ion internal energy (applied in this work) and (ii) the measurement of KER in the fragmentation of lifetime-selected ions, i.e., in MIKES experiments [15].

2.4. Calculation of the kinetic energy release

If one prepares a diatomic molecule with an excess energy E_{exc} above its dissociation threshold, the entire excess energy will be released into translational energy of the atomic fragments. For the fragmentation of polyatomic molecules only part of the excess energy is released into product translations, another part is channeled into product rotation and vibration (or electronic excitation) according to $E_{exc} = E_{vib} + E_{rot} + E_{trans}$. Haney and Franklin [46] proposed an empirical formula which describes the variation of the average KER with the excess energy E_{exc} and the number of vibrational degrees of freedom N of the parent molecule.

$$\mathrm{KER} = \frac{E_{exc}}{0.44N} \quad (8)$$

This formula accounts for the fact that the KER will decrease with increasing number of vibrations. The factor of 0.44 represents an effective number of oscillators. This simple approach appears valuable, since it does not require the knowledge of any microscopic parameter of the molecule or cluster. In the current work, however, the KER calculated from Eq. (8) turns out to be significantly too large. Consequently, we will propose a modified Franklin equation (see Section 4).

The critical assumption in the Franklin approach and its modifications is the linear relation between excess energy and KER. A more detailed analysis must take into account that due to the quantization of vibrational and rotational energy the KER cannot vary linearly with the excess energy, particularly at small excess energies.

Here, Klots proposed a model correlating the excess energy in the ion with the average KER [47] via Eq. (9).

$$E_{\mathrm{exc}} = \frac{r-1}{2}kT^{\#} + kT^{\#} + \sum \frac{h\nu_i}{\exp(h\nu_i/kT^{\#}) - 1} \tag{9}$$

where $kT^{\#}$ is the average total KER into the products. The number of rotational degrees of freedom of the products is r, ν_i are the normal modes of the products. Eq. (9) is based on the assumption of a dissociating microcanonical ensemble, in which the products are formed with a characteristic temperature $T^{\#}$, where the average total KER is given by $kT^{\#}$. It takes into account the conservation of energy and approximately also the correlation between rotational degrees of reactants and products. Eq. (9) should be applicable for the dissociation of non-linear molecules and clusters in low rotational eigenstates [48]. The latter condition is fulfilled for the rotationally cold clusters studied in this work. For thermal reactions the explicit treatment of the angular momentum of the molecules (clusters) may be necessary.

Numerous studies aimed at the KER in the fragmentation of polyatomic ions by electron impact and photoionization have confirmed the validity of Eq. (9) [28]. In the current work we will also employ Eq. (9) by numerical solution for $kT^{\#}$. Since the primary cluster ions investigated in this work are all formed from neutral clusters with non-linear equilibrium geometry, most likely these cluster ions themselves will, at least on the temporal average, also be non-linear. Nevertheless, some of the cluster ions do have a linear equilibrium geometry. The analysis of the current data suggests, that the Klots equation (Eq. (9)) needs to be modified in the case of primary cluster ions with linear equilibrium geometry.

In order to further check the validity of the Klots model we also performed more sophisticated calculations based on statistical theories of unimolecular reaction rates. Here, we consider one single specific reaction channel leading to products with a kinetic energy release KER with a rate constant k (E; KER). In general this channel may compete with other reaction channels, and the probability $P(E_{\mathrm{exc}}; \mathrm{KER})$ that the dissociation of molecules with excess energy $E_{\mathrm{exc}} = E - E_0$ above the dissociation threshold leads to products with KER is given by (for a survey see [49]):

$$P(E_{\mathrm{exc}};\ \mathrm{KER}) = \frac{k(E;\ \mathrm{KER})}{\int_0^{E_{\mathrm{exc}}} k(E;\ \mathrm{KER})\,\mathrm{dKER}} \tag{10}$$

The function $P(E_{\mathrm{exc}}; \mathrm{KER})$ represents a complete kinetic energy distribution which can ultimately be compared to either experimental KER distributions or average KER values. Starting from this approach we have calculated complete KER distributions based on phase space theory (PST) as outlined by Bowers and coworkers [50,51]. These calculations take into account the conservation of angular momentum explicitly. They require detailed information on the structure, the vibrational frequencies and the rotational constants of the parent cluster. A more detailed description of the formulas employed in this work has been given elsewhere [52]. At this point we note that the KER distribution is ultimately calculated from Eq. (11)

$$P(\mathrm{KER}) = \int_0^{\infty} P(J)_{\mathrm{react}} P(E, J;\ \mathrm{KER})\,\mathrm{d}J \tag{11}$$

where P(KER) is the probability for forming products with a kinetic energy release KER. $P(J)_{\mathrm{react}}$ is the rotational state distribution of the parent cluster, and $P(E, J; \mathrm{KER})$ the probability that parent clusters with internal energy E and rotational angular momentum J lead to products with a kinetic energy release KER. KER is the total kinetic energy released into all products. Note, that E, respectively, E_{exc}, has been dropped on the left side of Eq. (11) for the sake of brevity. The probability $P(E, J; \mathrm{KER})$ is given by

$$P(E, J;\ \mathrm{KER})\,\mathrm{dKER} = \frac{F^{\mathrm{orb}}(E, J;\ \mathrm{KER})\,\mathrm{dKER}}{F^{\mathrm{orb}}(E, J)} \tag{12}$$

where F^{orb} (E, J, KER) is the flux through the loose (orbiting) transition state at total energy E and angular momentum J per unit KER, and $F^{orb}(E, J)$ is the total flux through this transition state. The flux mainly depends on the vibrational and rotational temperature of the parent cluster and the structure, particularly the rotational constants, of the products. The restriction to loose transition states is justified by the fact that only simple bond fissions are covered in this work. For details the reader is referred to the literature [50–52]. The molecular parameters used in the current calculations are listed in the Appendix A.

2.5. Ab initio calculations

The experiments and their analysis described in this review are complemented by quantum chemical calculations. These calculations concern the equilibrium structures of the relevant clusters, their vibration frequencies and rotational constants, which are required for the PST calculations. We will also compare the experimental ionization energies and dissociation energies to values calculated directly by ab initio techniques. In the following we briefly mention the techniques and levels of computation employed.

All ab initio calculations were performed employing the Gaussian program package. Over the years different versions from Gaussian'90 [53] to Gaussian'98 [54] were used. All the calculations performed start with a full geometry optimization without any symmetry constraints, followed by normal coordinate analysis. The SCF calculations (self-consistent field) are based on UHF wave functions (unrestricted Hartree Fock) [55]. Post-SCF calculations were performed at different levels from MP2 [56] (second-order Möller–Plesset perturbation theory) to the QCISD method [57] (quadratic configuration interaction with singles and doubles) and CCSD [57] (coupled cluster). For some of the equilibrium structures a population analysis was performed in order to get an estimate of the spin and the charge distribution [58,59]. Throughout the work many different basis sets were employed ranging from the standard 6-31G* to the triple zeta basis set aug-cc-pVTZ [60]. The accuracy of ab initio calculations is inherently difficult to discuss. However, in general bond length calculated at the MP2/6-31G* level will be accurate to within 0.02 Å [61]. The accuracy is estimated to be on the order of 1–2° for bond angles, and 100 meV for energies. In a comparative study of molecules containing first and second row elements the best results were obtained at the MP4 or the QCISD level with a 6-311G(2df,2pd) basis set [62].

3. Experimental aspects

In the following we describe the experimental set-up of the photoelectron–photoion coincidence spectrometer employed in this work [43,63–65]. It consists of an electron spectrometer, and an ion time-of-flight spectrometer. The sample introduction and the light source will also be discussed briefly.

3.1. The electron spectrometer

For energy selection of the ions we employ electron analyzers which preferentially transmit electrons with zero kinetic energy. The simplest type of zero volt or threshold electron analyzers is an angular discriminator, which was first described by Baer et al. [66]. This angular discriminator consists of a simple tube with an aperture at the entrance and more important at the exit. In the case of small electric fields, threshold electrons are transmitted through this analyzer but electrons with significant kinetic energy are discriminated against. The basis of this effect is that the trajectories of electrons depend on their initial kinetic energy. The theoretical description of angular discriminators has been described by various authors [66–68]. The critical aspect is the ratio of the length of the analyzer to the diameter of the exit aperture. For the analyzer employed in this work this ratio is 30:1. The second important contribution to the overall resolution is the ratio of the initial kinetic energy of the electron to the total energy gained during the acceleration in the ion source towards the threshold analyzer. A high resolution of the analyzer, i.e., a good

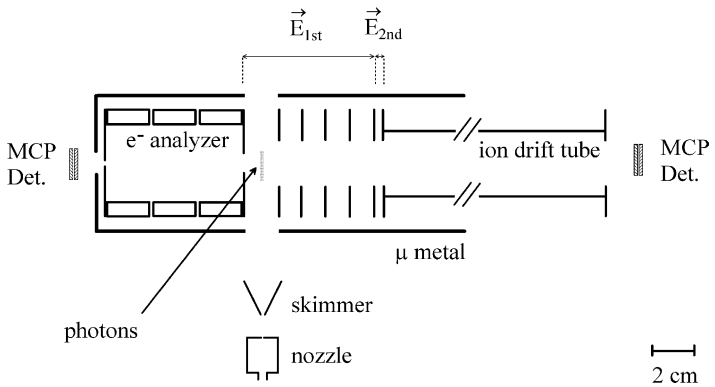

Fig. 2. Experimental set-up of the coincidence spectrometer including the electron and the ion spectrometer. Adapted from [65].

discrimination of kinetic electrons requires a small energy gain. The inherent problem of angular discriminators is their asymmetric instrument function. Due to the fact that there is no angular discrimination for kinetic electrons running on the spectrometer axis this instrument function exhibits a 'hot electron tail' [67]. As mentioned the original design of an angular discriminator was based on a straight tube. An even better performance is observed when replacing the long tube by three short tubes. In the current set-up we used three cylindrical lenses of 2 cm length with an exit aperture of 2 mm diameter (see Fig. 2). These three lenses are independently supplied with voltages, with the middle one serving for refocusing the threshold electrons. Low energy electrons are very sensitive to stray magnetic fields, e.g., originating from the earth. In order to shield the electron spectrometer from such fields the spectrometer is surrounded by a micrometal cylinder, which decreases external fields by a factor of 400:1. All experiments discussed in this review have been performed employing homogeneous static fields of 20–30 V/cm in the ion source.

The typical energy resolution of the experiment is best illustrated by looking at the photoelectron spectra of rare gas atoms. As an example Fig. 3 shows the threshold (0 V) photoelectron spectrum (TPES) (upper curve) and the photoionization efficiency (PIE) spectrum (lower curve) of the argon atom. The argon cation has a ^{2}P electronic ground state, which is split into two components by spin–orbit coupling ($^2P_{3/2}$ at 15.760 eV and $^2P_{1/2}$ at 15.937 eV [69,70]). The splitting energy is 0.177 eV. Starting from the neutral ground state of the atom there are two Rydberg series (*s* and *d* series) converging to each of the spin–orbit states. In the case of the upper spin–orbit state, the notation *s*′ and *d*′ is common. Those members of the *s*′ and *d*′ series located above the $^2P_{3/2}$ state can

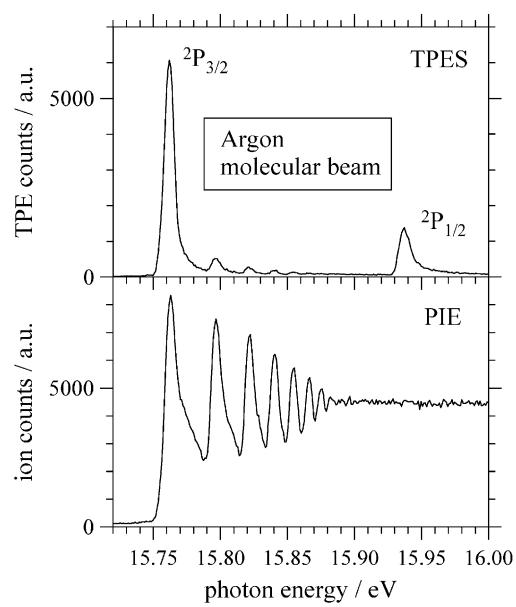

Fig. 3. Threshold (0 V) photoelectron spectrum (TPES) and photoionization efficiency curve (PIE) of argon. The intensity maxima in the PIE spectrum are dominated by Rydberg states *ns*′ with $s \geq 11$.

autoionize by ejection of an electron, with an kinetic energy given by the relevant energy difference. The Franck–Condon factors for Rydberg excitation are significant and dominate the entire PIE spectrum. The optical resolution in Fig. 3 is on the order of 6 meV. At higher optical resolution the s' and d' series can easily be distinguished [71].

There is one peculiarity in the argon spectra. One member of the s' series, i.e., the $11s'$ state, is accidentally almost degenerate with the ion ground state. It is located just 3 meV above the $^2P_{3/2}$ state. Since the Franck–Condon factor for Rydberg excitation is larger than that for direct ionization, the maximum in the PIE curve is due to the $11s'$ Rydberg state at 15.763 eV. In a perfect TPES, no signal should be observed at 15.763 eV, since the photoelectrons produced at that excitation energy must have a kinetic energy of 3 meV. In the TPES shown here, the maximum does also occur at 15.763 eV, indicating a resolution slightly worse than 3 meV. In the region of the $^2P_{3/2}$ state the ionization efficiency is modulated by the absorption into Rydberg states converging to the upper spin–orbit state. This region is thus not well suited for discussing the energy resolution of the electron analyzer. Here, it is better to look at the region of the $^2P_{1/2}$ state. There, the ionization cross-section is basically independent of the excitation energy. The TPES in the region of the $^2P_{1/2}$ state directly gives the instrument function of the electron spectrometer. This function includes contributions from the electron analyzer as well as the optical resolution of the light source.

It is common practice to characterize the energy resolution of a spectrometer by the full-width at half-maximum of the instrument function, which is typically 20 meV in the current experiments. However, due to the asymmetry of the transmission function, the instrument function is also asymmetric. Therefore, it is important to characterize this 'hot electron tail.' This is, e.g., possible by specifying the relative amount of electrons observed at a certain energy, e.g., directly below the second ionization threshold ($^2P_{1/2}$). This is typically on the order of 3–4% in the current experiment. Another useful indication is the intensity ratio of the $^2P_{1/2}$ peak to the $12s'$ (15.797 eV) or $13s'$ peak (15.822 eV). A good discrimination of 'hot electrons' is concluded from a ratio of $^2P_{1/2} : 12s' > 2 : 1$, as is the case in Fig. 3. For the sake of completeness we mention that some groups employ post-analyzers in order to reduce the hot electron tail. A significantly higher electron energy resolution is today also easily achieved, e.g., by the penetrating field technique [72,73] and the pulsed field ionization technique [19,74,75]. However, all these techniques are based on inhomogeneous fields and thus not well suited for kinetic energy release measurements. Nevertheless, we note, that we were recently able to measure the KER in the dissociative ionization of oxygen [76] in a pulsed field (PFI-PEPICO) experiment.

3.2. The ion time-of-flight mass spectrometer

The aim of the current experiment requires an ion analyzer capable of providing a sufficient mass resolution and kinetic energy resolution. In a coincidence experiment this is best achieved by using a linear time-of-flight mass spectrometer [77] of the Wiley–McLaren type [78]. The crucial parameter is the electric field gradient in the ion source. Here, a high field in general increases the mass resolution. A low field, on the other hand, improves the discrimination against energetic electrons and thus the internal energy resolution of the parent cluster ions. At the same time a low field increases the width of the ion TOF distributions and thus the sensitivity for small kinetic energy release. The current set-up of the ion TOF analyzer consists of a long first acceleration region of 5 cm and a short second acceleration region of 3 mm. The field in the first region is typically smaller than 30 V/cm, that in the second region about 400 V/cm. The ion TOF-mass spectrometer is schematically illustrated in Fig. 2. Further details have been reported elsewhere [65].

For illustration of the kinetic energy resolution, Fig. 4 shows a typical ion time-of-flight spectrum of argon recorded with a thermal sample. From the FWHM of 174 ns one derives a translational temperature of 302 K, which agrees with the actual laboratory temperature. Note that this corresponds to about

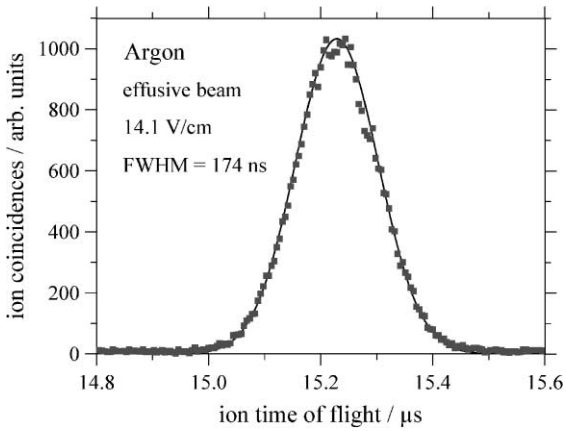

Fig. 4. TPEPICO ion time-of-flight spectrum of argon, recorded at ionization energy (15.760 eV) in an effusive beam, i.e., at 300 K.

40 meV kinetic energy. The KER resolution is in general on the order of 10 meV.

3.3. The sample introduction

The sample is introduced by means of a supersonic molecular beam obtained by expansion through small circular nozzles [79,80]. Here we make use of the fact that the internal degrees of motion are significantly cooled in the supersonic expansion [81,82] eventually leading to condensation, i.e., cluster formation.

In general the temperature is not a well-defined quantity in a molecular beam. For that reason we had earlier developed a technique which allows to determine the average internal energy of the molecules in a supersonic beam [83]. More important for the current experiment is the translational (kinetic) energy of the molecules (clusters). The kinetic energy of the molecules along the beam axis is larger than in a thermal sample, however, the distribution of kinetic energies is narrow. Even lower is the transverse translational temperature. In general the order of temperatures is $T_{\mathrm{vib}} > T_{\mathrm{rot}} \gg T_{\mathrm{trans}\,||} > T_{\mathrm{transl}\,\perp}$. In our experiment the low transverse translational temperature has the additional advantage of improving the mass resolution of the TOF-MS, since beam axis and TOF axis are perpendicular. This is due to the fact that the FWHM scales with the square root of the kinetic energy of the molecules (cf. Eq. (5)).

Theoretical models for describing the cooling of molecules in a supersonic expansion have been described extensively [79]. At this point we only briefly recall a simple estimate of the translational temperature of a supersonic beam of atoms given by Anderson and Fenn [84]. According to this the terminal Mach number, i.e., the ratio of actual velocity to local sound velocity is given by Eq. (13), where p_0 is the stagnation pressure (bar) and d is the nozzle diameter (cm), c is a constant which for argon takes the value 135. For parameters typical for the experiments of this work ($p_0 = 2$ bar, $d = 0.005$ cm) one arrives at $M_{\mathrm{t}} = 21$.

$$M_{\mathrm{t}} = c(p_0 d)^{0.4} \tag{13}$$

The cooling in a supersonic expansion is usually reported as the ratio of the actual translational temperature over the nozzle temperature T_0 as given in Eq. (14), where the ratio of the heat capacities $\gamma = c_p/c_v$ is 5/3 for a mono-atomic gas. Combined with the terminal Mach number this would lead to a terminal temperature of 2 K. In general the actual temperature in our experiments is somewhat larger.

$$\frac{T}{T_0} = \frac{1}{1 + (\gamma - 1)/\gamma M^2} \tag{14}$$

Besides from the cooling of internal degrees of freedom, which is very important for investigating isolated molecules, molecular beams also give access to clusters. The formation of clusters in supersonic beams has been extensively discussed in the literature [85–88]. In the current work we only touch the subject of van der Waals clusters and present a simple estimate of the average cluster size according to Wörmer et al. [89]. This average cluster size can be calculated from Eqs. (15) and (16). Here, d is the nozzle diameter (cm), p_0 the stagnation pressure (mbar) and T_0 the nozzle temperature (K). The constant k is 1646 for argon. For our typical expansion conditions we arrive at an estimated average cluster size of 6. The experiments described in this work suggest that the actual average cluster size is even smaller.

$$N = 2.1 \times 10^{-4} (\Gamma^*)^{1.95} \tag{15}$$

with

$$\Gamma^* = \frac{kd^{0.85}p_0}{T_0^{2.29}} \quad (16)$$

Typical stagnation pressures in the current experiments range from 0.5 to 10 bar. Most experiments used circular nozzles with open diameters between 20 and 100 μm, some of the experiments a conically diverging nozzle. The nozzles are all metal (platinum), allowing to be operated between 200 and 400 K. The supersonic beam was skimmed by home-made skimmers with opening 500 μm. The typical distance skimmer nozzle was varied between 5 and 20 mm. Ion TOF spectra illustrating typical cluster distributions are shown in the next section (e.g., Fig. 6 for an Ar cluster beam).

3.4. The electron ion coincidence experiment

As pointed out earlier the energy selection of cluster ions is based on the condition that only one pair of photoelectron and photoion is formed at a time. Both particles are detected in their respective spectrometer. The key point is that the ion time-of-flight measurement is triggered by the detection of an electron. This ensures the coincidence condition. Combination with Eq. (1) then yields the internal energy of the ion under investigation. This forms the basis for all electron ion coincidence experiments.

It is important to note that the acceptable count rate for coincidence events (more precisely the total ionization rate) must not exceed the inverse of the ion time-of-flight. Otherwise false coincidences would blur the true coincidences. In the current experiments the coincidence count rate of the clusters was typically smaller than 1 count per second. For a description of the relation between electron, ion and coincidence count rate on one hand and the relevant collection efficiencies and the total ionization rate on the other the reader is referred to the literature [16]. The entire TPEPICO spectrometer including the electron analyzer and the ion TOF-MS is shown in Fig. 2. All time-of-flight spectra displayed in this review are coincidence spectra.

3.5. Light sources

The experiments described in this review require continuously tunable vacuum ultraviolet (VUV) radiation. A very powerful source of VUV radiation are electron storage rings, which emit synchrotron radiation (SR) in the range from the infrared to the hard X-ray region [90–92]. All experiments described here utilize SR provided by the electron storage ring BESSY I in Berlin. The BESSY storage ring had a circumference of 62.4 m and was in general operated at an electron energy of 800 MeV. The SR was dispersed at the 3 m NIM 1 beamline [93]. Typically the experiments discussed in this work were operated at a photon resolution of 5–10 meV. The advantage of SR over other laboratory light sources (lasers, discharge lamps, etc.) mainly lie in the continuous tunability over several hundred electron volts. For the purpose of the current experiment, the SR source may be considered quasi-continuous in the time domain. A description of the standard techniques in VUV spectroscopy can be found in the book by Samson [94].

4. Results and discussion

In the following sections we will review investigations of the KER in the dissociative formation of five small cluster systems, three homogeneous clusters [Ar_2^+, $(CO)_2^+$, $(N_2)_2^+$] and two heterogeneous clusters [$ArCO^+$, ArN_2^+]. In each case we will start with a brief review of information available from the literature, before describing investigations from our own laboratory.

4.1. Argon cluster: the formation of Ar_2^+

The Ar_2^+ ion is certainly one of the most extensively investigated dimer ions. Today very accurate information is available on the adiabatic ionization energy of the neutral dimer and the binding energy of the Ar_2^+ ion, respectively. This system may thus well serve as a test case for the translational energy

spectroscopy described in this review. In the following we will briefly review the known information on the neutral dimer and trimer before proceeding with the corresponding ions. An interesting review of neutral and ionic rare gas clusters – including argon clusters – has been published by Last and George [95].

Experiments [96] and theory [97] agree that the equilibrium distance in the neutral argon dimer is about 3.8 Å. From absorption spectra the vibrational frequency has been derived as 31 cm^{-1} [98], i.e., extremely low. The experimental binding energy of the neutral dimer is $D_0 = 10$ meV [99–101]. Ab initio and dynamics calculations show that the neutral trimer has the equilibrium geometry of an equilateral triangle [26,102] with the length of its edge being about 3.8 Å [103,104]. The binding energy of neutral Ar_3 with respect to the atoms is 20 meV [105], i.e., just twice that of the dimer.

The properties of the Ar_2^+ ion and the Ar_3^+ ion are distinctly different from those of their neutral counterparts, particularly with respect to the equilibrium geometry, but also the binding energy. This will be of pivotal importance for most investigations in this work. Most of the experimental and theoretical investigations report an equilibrium distance in the Ar_2^+ ion between 2.41 and 2.529 Å. For a compilation of data see [106,107]. More recent experimental work by Signorell and Merkt [108] arrive at $r_e = 2.32 \pm 0.09$ Å, which is about 1.5 Å less than in the neutral Ar_2. The experimental vibrational frequency in the Ar_2^+ ion is about 310 cm^{-1} [108–111]. Theoretical values range from 293 to 320 cm^{-1} [106,107,112,113]. The equilibrium geometry of the Ar_3^+ ion has received a lot of interest in recent years. The most valuable information is coming from ab initio calculations. Early work considered a triangular equilibrium geometry [114], and an unsymmetrical linear geometry [115]. More recent investigations, however, unanimously agree on a symmetric linear structure [27] with two identical bond lengths. In any case, the potential energy surface is certainly very shallow towards non-linearity. The degenerate bending mode of symmetric, linear Ar_3^+ ions has a frequency of about 20 cm^{-1}. For the bond length of symmetric linear Ar_3^+ values between 2.59 and 2.67 Å [27,103,116–119] have been obtained from calculations. Molecular dynamics calculations predict that Ar_3^+ is a very floppy molecule with efficient intramolecular vibrational energy redistribution and an early onset of chaotic dynamics [120]. The difference in the equilibrium geometry of neutral and ionic argon trimers may be important for many experiments, since any Ar_3^+ formed directly from neutral Ar_3 will on the temporal average certainly be nonlinear.

The measured values for the ionization energy of neutral Ar_2 span a range from 14.44 [121], 14.45 [122], 14.50 [123], 14.518 [124], 14.52 [125] to 14.53 eV [126]. The most accurate values currently available for the IE of the argon dimer have been derived from pulsed field ionization spectroscopy with 14.4556 ± 0.0008 eV [108] and 14.4572 ± 0.0007 eV [127]. The binding energy of the dimer ion was derived as $D_0 = 1.3147$ [108] and 1.3130 eV [127]. For the ionization energy of the argon trimer values of 14.33 [123], 14.35 [124] and 14.42 eV [126] have been reported. Combining these numbers with the information available for the neutral clusters one arrives at a picture of the argon cluster energetics as depicted in Fig. 5.

The photoelectron and PEPICO spectra of an argon cluster beam are basically structureless [124,128], if the average cluster size is large. This was interpreted as a hint for dissociative ionization of larger clusters. By reducing the average cluster size Norwood et al. [124] obtained a TPEPICO spectrum, which was believed to be dominated by contributions from Ar_2. A high resolution PIE measurement was reported by Dehmer [129]. Due to the absence of any energy selection of the ions, this spectrum was most likely contaminated by autoionization structure from the neutral dimer. Finally the photodissociation of Ar_2^+ ions [121,130] and Ar_3^+ ions [131–134] has been investigated in the UV range by various groups.

Cluster beams are in general characterized by a distribution of cluster sizes, which depends on the expansion conditions. In order to get an estimate of this cluster distribution, Fig. 6 shows the TPEPICO-TOF mass spectrum of an argon cluster beam recorded

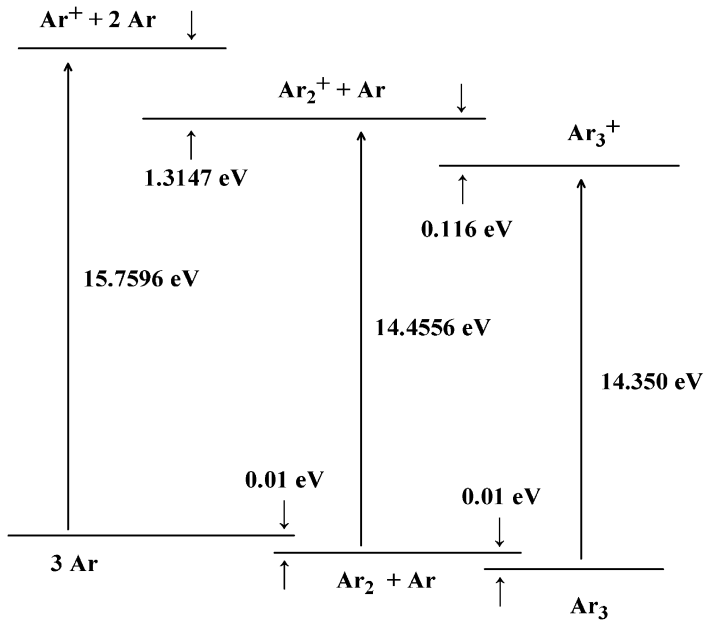

Fig. 5. Thermochemistry of the argon cluster systems according to [99,108,124].

during a scan of the photon energy between 14.66 and 15.67 eV [135]. The dominating ion is the dimer ion. It is important to note that there is extremely little trimer ions to be observed. As the reader will see, this does not mean there are no neutral trimers in the cluster beam but most of the neutral trimers can only be ionized dissociatively. Experimental details of this study are given elsewhere [135].

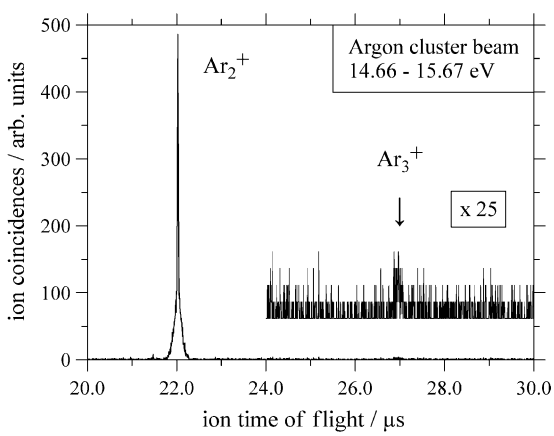

Fig. 6. TPEPICO-TOF spectrum of the argon cluster beam recorded during the wavelength scan indicated.

In Fig. 7 four TPEPICO-TOF spectra of the Ar_2^+ ions recorded with significantly higher time resolution at the photon energy indicated are displayed. At all photon energies the TOF distribution consists of a narrow and a broad component. In addition to the experimental data (symbols) the plots also show simulated ion TOF distributions. These simulations are based on the sum of two Gaussian functions with the indicated FWHM. The FWHM of the narrow component turned out to be independent of the photon energy. The width of the broad component, however, increases significantly with increasing photon energy. This can easily be rationalized by the conclusion that the narrow component is due to the non-dissociative ionization of argon dimers. The analysis of the FWHM (18 ns) according to Eq. (5) yields a temperature of 6 K, which is just the transversal translational temperature of the cluster beam. The FWHM of the broad component, on the other hand, correlates with kinetically warm argon dimer ions. The only

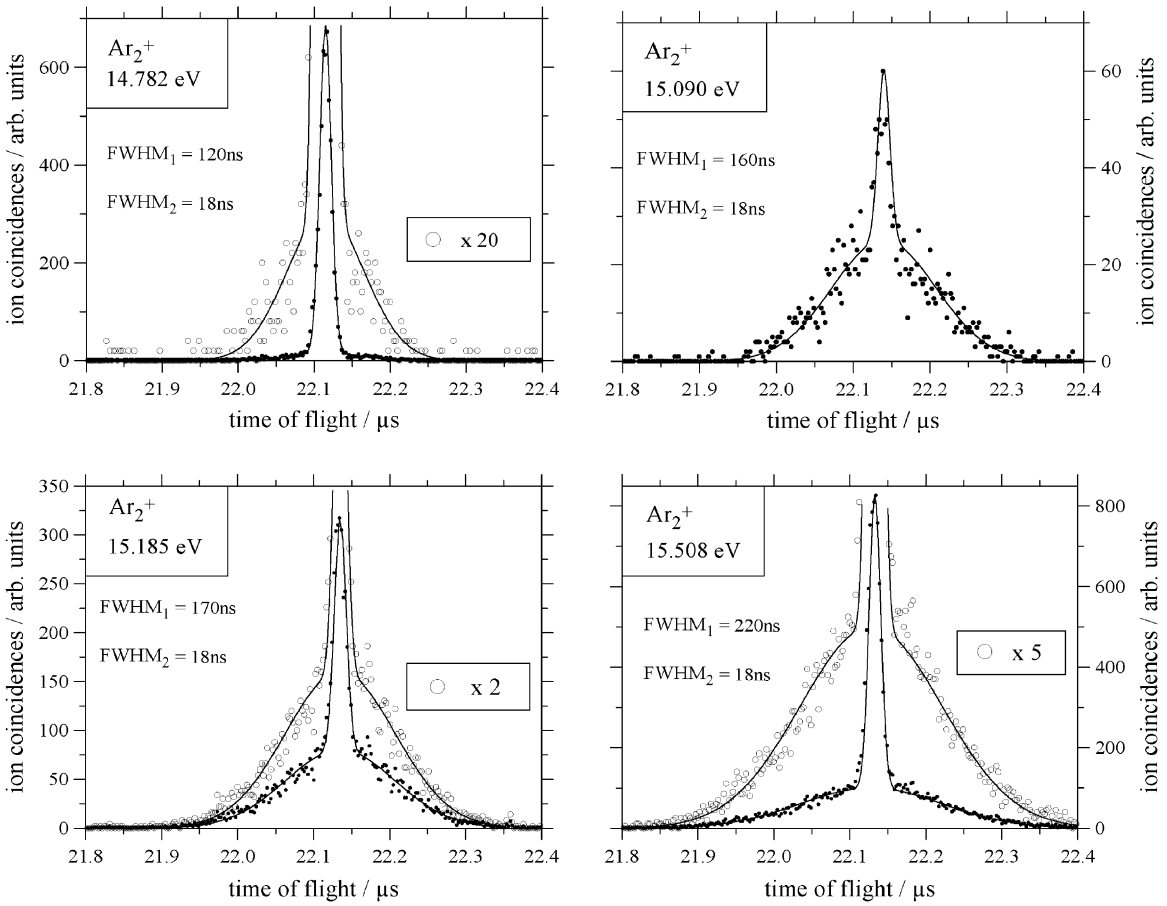

Fig. 7. TPEPICO-TOF spectra of Ar_2^+ ions at various photon energies. Symbols: experimental data; lines: simulation [135].

reasonable origin for the latter is the formation by dissociative ionization of a larger cluster as indicated in Eq. (17).

$$Ar_3 + h\nu \rightarrow Ar_3^+ + e^- \rightarrow Ar_2^+ + Ar + e^- \qquad (17)$$

Deriving the average experimental KER into the Ar_2^+ from the TOF spectra requires an assumption of the parent cluster. Assuming that the kinetically hot Ar_2^+ ions are due to the dissociative ionization of neutral Ar_3 this KER can be calculated employing Eq. (7). For the energy range covered the experimental KER(Ar_2^+) varies between 5 and 120 meV. This KER is plotted in Fig. 8 as a function of the photon energy (upper *x*-axis). The release of kinetic energy in the dissociative ionization of argon clusters has also been studied by Furuya and Kimura [32], however not as systematically. For low stagnation pressure their results in general agree with ours.

In our original work [135] the analysis of the theoretical KER was based on the original Klots equation Eq. (9) for the reactive process given in Eq. (17), i.e., we assumed a non-linear geometry of the Ar_3^+ ion. In the numerical solution of Eq. (9) we took into account that the product ion Ar_2^+ has two rotational degrees of freedom ($r = 2$) relevant for Eq. (17) and a vibrational frequency of 310 cm^{-1} [109–111]. This KER(Ar_2^+) calculated for the statistical decay of Ar_3^+ ions is also shown in Fig. 8 as a function of the excess energy E_{exc} (lower *x*-axis). The comparison of theoretical and experimental KER curves requires an assumption

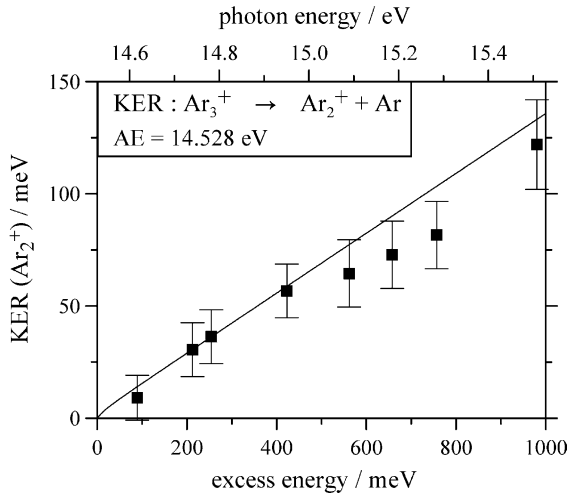

Fig. 8. Average experimental (symbols) and theoretical KER(Ar_2^+) (line) according to Eq. (9) for the process indicated [135]. The threshold energy was assumed to be 14.528 eV relative to neutral Ar_3.

regarding the threshold energy of the underlying reaction. In practice the two curves are shifted against each other until agreement is obtained. The photon energy for which the KER becomes zero corresponds to the adiabatic threshold energy (appearance energy, AE) for the dissociative formation of Ar_2^+ ions by reaction Eq. (17). Here, we first used a value of AE = 14.528 eV [135]. As indicated in Fig. 6, this threshold energy is related to the adiabatic IE of the argon dimer by Eq. (18), where the binding energy of the neutral trimer with respect to the loss of one argon atom is BE(Ar_3) = 10 meV. This led to an adiabatic IE of the argon dimer of 14.518 eV, which was compatible with the value reported by Norwood et al. [124]. By combination with the well known IE of the argon we arrived at a binding energy of the dimer ion of BE(Ar_2^+) = 1.252 eV. A close inspection of Fig. 8 shows that the calculated KER curve is somewhat steeper than the experimental data.

$$AP(Ar_2^+) = IP(Ar_2) + BE(Ar_3) \quad (18)$$

In the context of another system discussed below, the $ArCO^+$ [52], we complemented our Klots analysis by a more sophisticated PST analysis, which properly takes into account the geometry of all species and the conservation of angular momentum. We have now also calculated the theoretical KER(Ar_2^+) in pure argon clusters by the PST approach. In these calculations we assumed a vibrational temperature of the cluster beam of 40 K and a translational and rotational temperature of 27 K. The resulting KER is plotted again together with the experimental data in Fig. 9. We note, that the assumptions made for the temperature of the cluster beam are not very critical. Changing, e.g., the rotational temperature by 20 K changes the average KER by less than 1 meV. As it turned out agreement between experimental and theoretical data was now only obtained when assuming an appearance energy of 14.49 eV. In analogy to the procedure described this leads to an adiabatic IE of Ar_2 of IE(Ar_2) = 14.480 ± 0.05 eV, and a binding energy of the dimer ion of BE(Ar_2^+) = 1.290 ± 0.05 eV. The difference between this new value and the old value derived from Fig. 8 (IE = 14.518 eV) [135] amounts to 38 meV, which is small but significant.

What is the reason for the discrepancy between the PST and the original Klots calculation? For this we have to recall the assumptions made by Klots in his

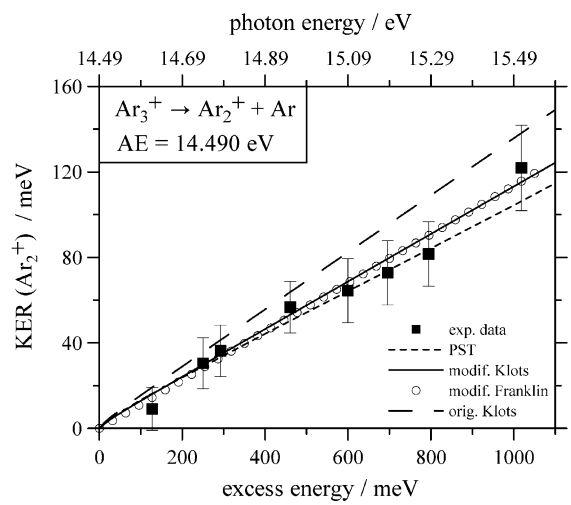

Fig. 9. Comparison of average experimental KER(Ar_2^+) with four different calculations. Note that the modified Klots and the modified Franklin calculations are hardly distinguishable. The threshold energy was assumed to be 14.490 eV relative to neutral Ar_3.

seminal papers. There he was dealing with a microcanonical ensemble of molecules prepared with a particular excess energy which is then distributed over the degrees of freedom of the products. The Klots equation does not take into account the conservation of angular momentum explicitly, but it accounts for the correlation between certain degrees of freedom. In the dissociation of a non-linear molecule one of the rotational degrees of the products is then excluded from the calculation, since it does not correlate with one of the reactant vibrations. The Ar_3^+ ion, however, has a linear equilibrium geometry. In the dissociation of Ar_3^+ both external rotors of the Ar_2^+ product correlate with a bending vibration in the Ar_3^+. But then there is no point in excluding one of the product rotors from the Klots calculation. We thus conclude that the original Klots equation (Eq. (9)) is not applicable for linear parent molecules. For calculating the KER in the dissociation of a linear molecule we suggest a modified Klots equation (Eq. (19)), which does not exclude any product rotors. That part of the total KER calculated from Eq. (19) which is observable in the Ar_2^+ is also plotted in Fig. 9. Evidently the modified Klots calculation is in very good agreement with the threshold energy of 14.49 eV. The comparison of the KER curve from the original and the modified Klots equation reveals that the slope of the ladder is significantly smaller than that of the former. This is a direct consequence of the additional rotor in Eq. (19) which decreases the KER. The calculation based on the original Klots equation was also presented because in our experiment the Ar_3^+ ions are formed by vertical excitation, which certainly leads to a non-linear conformation. The comparison of the PST calculation (Fig. 9) and the two Klots calculations (Eqs. (9) and (19)) leads to the conclusion, that the dissociation of the Ar_3^+ ion is dominated by its linear equilibrium geometry.

$$E_{\mathrm{exc}} = \frac{r}{2}kT^{\#} + kT^{\#} + \sum \frac{h\nu_i}{\exp(h\nu_i/kT^{\#}) - 1} \quad (19)$$

In the methods section we have pointed out that the KER in a dissociative ionization of a molecule has often been successfully calculated from an empirical formula introduced by Franklin (Eq. (8)). The short coming of that formula is the linear relationship between the excess energy and the KER. Due to the quantization of rotational and vibrational energy levels this linearity cannot be appropriate for small excess energies. On the other hand, e.g., the modified Klots curve shown in Fig. 9 does not exhibit a pronounced deviation from linearity. What is more important, is that the KER calculated from Franklin's formula (Eq. (8)) is systematically too large. A reasonably good agreement between calculated and experimental KER is, however, observed, if Eq. (8) (after transformation to $\mathrm{KER}(Ar_2^+)$) is scaled by a factor of 0.6 ± 0.1. This leads to a modified Franklin equation as given in Eq. (20). For illustration the KER calculated from Eq. (20) is also shown in Fig. 9. Note that at excess energies above 100 meV the modified Franklin and the modified Klots calculation are basically indistinguishable. Only at excess energies smaller than 100 meV a difference between the two calculations is discernible, since the Klots approach exhibits deviations from linearity in this region.

$$\mathrm{KER}(D^+) = 0.6\frac{M_{\mathrm{N}}}{M_{\mathrm{P}}}\frac{E_{\mathrm{exc}}}{0.44N} \quad (20)$$

Although the original Franklin equation and the modified Franklin equation are purely empirical equations, they are quite helpful, particularly in situations where no information on the vibrational frequencies of the parent cluster are known. We will encounter this situation when discussing the properties of the $(N_2)_2^+$ ion. Since no sufficient structural information is available for that system, the theoretical KER can at this point only be calculated by the use of Eq. (20). We wish to point out, that Eq. (20) has been tested for all other reactions discussed in this work against PST and Klots calculations and found to yield surprisingly good results. The physical interpretation of the original Franklin equation was in general based on the picture that on the average only 44% of the oscillators are effective in the dissociation. While that equation has originally been set-up for molecules, in the current work we are dealing with parent cluster ions, which in general have additional low frequency

vibrational modes (intermolecular modes) compared to typical molecules. The very good agreement observed employing Eq. (20) seems to indicate that the number of effective oscillators is significantly higher for clusters (73%) compared to molecules (44%).

The best value for the adiabatic IE derived for the argon dimer in this work is 14.480 ± 0.05 eV corresponding to a binding energy of the Ar_2^+ of 1.290 ± 0.05 eV. Within the error limits of our analysis this is compatible with the most accurate data available [108] (14.4556 and 1.3147 eV). The IE derived in this work is 40 meV higher than the value of 14.44 eV determined by Moseley et al. [121]. The latter investigation employed a kinetic energy analysis of the atomic products in the photodissociation of thermalized Ar_2^+ ions, thus a method similar to the one employed in this work. On the other hand our improved value for the IE is about 40 meV smaller than the value determined by Norwood et al. [124]. Since Norwood et al. performed photoionization of an argon cluster beam at a relatively low stagnation pressure of 60 Torr, one may expect to see only little contribution from larger clusters. What is more important in this case is the influence from poor Franck–Condon factors for ionization at the adiabatic IE. Since the geometry of both the neutral dimer and trimer is distinctly different from that of the corresponding ion, ionization is hardly possible at the adiabatic IE. This is reflected in the fact that even in the best PFI-PE spectra available [108,127] the first vibrational state of the Ar_2^+ ion observed is the $v = 3$ state. Indeed the correct assignment of the vibrational progression observed in the electron spectrum appears problematical. Hall et al. [122] reported two different IE values based on different assignment of vibrational states. Interestingly the difference of 40 meV mentioned almost exactly corresponds to one vibrational quantum in the Ar_2^+ ($310\,cm^{-1}$) and is thus relevant for the vibrational assignment of the photoelectron spectra. The fact that Moseley et al. [121] and our value bracket that of Signorell and Merkt [108], and Onuma et al. [127] gives additional support to the latter.

So far the average KER was the only result of the phase space calculations discussed. Obviously those

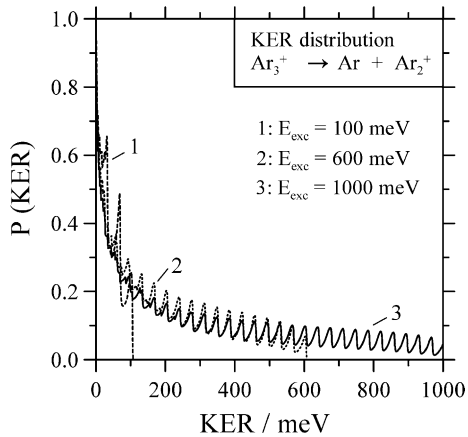

Fig. 10. Kinetic energy release distributions for the dissociative formation of Ar_2^+ at different excess energies.

calculations yield much more information. In fact the PST calculations according to Eq. (11) lead to the complete KERDs. For the dissociative formation of Ar_2^+ these KERD are shown in Fig. 10 for different excess energies. The main result is that the KERD is in all cases thermal, i.e., the most probable KER is KER = 0. Interestingly all three KERD displayed exhibit pronounced oscillations with the period of the vibrational energy spacing. Thermal KERDs are also observed for all other systems discussed in this work. It is also interesting to see which rotational angular momentum of the parent cluster contributes to the flux into the products. This flux depends on the excess energy and on the actual kinetic energy release. As an example Fig. 11 shows this flux for an excess energy of 1000 meV and for different KER. A low KER at $E_{exc} = 1000$ meV implies that much of the flux has to go through high J states, while if the KER approaches the excess energy the flux can only go through low J states. Note that the flux for high KER appears to be bimodal. This is expected to have important implications for the rotational state distributions of the product ions.

Due to the low Franck–Condon factors for direct (non-dissociative) ionization, the threshold photoelectron spectrum as well as the total Ar_2^+ ion yield spectrum recorded in an argon cluster beam will in general be contaminated by contributions from

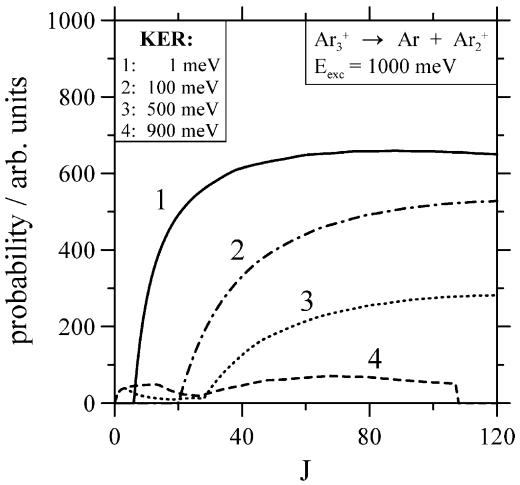

Fig. 11. Probability for observing Ar_2^+ with a specific kinetic energy release KER as a function of the rotational angular momentum J of the Ar_3 cluster ($E_{exc} = 1000$ meV).

dissociative ionization of larger clusters. This opens the question: what is the true molecular ionization spectrum of neutral argon dimers? One way to access this Ar_2 spectrum is to record a high resolution TPE spectrum or a PFI spectrum in a very dilute molecular beam as was done by Signorell and Merkt [108] and Onuma et al. [127]. Although these spectra represent the best data available for the Ar_2, one short coming is that contributions from other cluster beam components cannot be ruled out in a pure electron spectrum. In principle one could also try to mass select neutral Ar_2, e.g., by scattering techniques, and then record the ionization spectrum. A completely different approach was presented in our previous work [135]. There a time-of-flight gate was applied to the Ar_2^+ TOF spectrum collecting only those ions arriving at the detector within a small time interval (20–50 ns) centered at the TOF of the Ar_2^+ ions formed by non-dissociative ionization. This introduces a kinetic energy discrimination which highly favors signal from non-dissociative ionization but discriminates against dissociative ionization originating from larger clusters.

In the previous section we showed the formation of kinetically hot Ar_2^+ ions by dissociative ionization of neutral Ar_3. Ar_3^+ ions, however, are not observed with significant intensity in the energy range covered. This is neither due to a possible kinetic shift (all ion signals are strictly symmetric) nor due to a mass discrimination of the TOF spectrometer. The energy range covered in our work ($h\nu > 14.528$ eV) is already above the dissociation threshold of the Ar_3^+ ions. Since the dissociation energy of Ar_3^+ ions is relatively small (0.12 eV) and the experiment is performed under cluster beam conditions, i.e., at low rotational temperature, we do in fact expect that all intermediate Ar_3^+ ions will dissociate on the time scale of the experiment (several 100 ns). This is in agreement with the work of Buck and coworkers [136,137], where only Ar^+ and Ar_2^+ ions, but no Ar_3^+ ions, are observed in the 70 eV electron impact ionization of mass-selected Ar_3 clusters. The latter experiment did not employ energy selection of the ions. Thus, in principle, one might expect to observe Ar_3^+ ions in the mass spectrum, if those are formed with an internal energy below the dissociation threshold. The probability for this seems to be small. Such a contribution to the ion signal cannot happen in our experiment due to the threshold electron selection. We have to conclude that the observation of Ar_3^+ ions in some EI experiments is due to the dissociative ionization of even larger clusters. If the formation of Ar_3^+ ions is caused by successive evaporation of several argon atoms from a large cluster, the rotational temperature of the intermediate cluster ions can increase significantly. This can lead to very small rate constants and to the observation of metastable decay in magnetic mass spectrometers [24,138].

4.2. Carbon monoxide cluster: the formation of $(CO)_2^+$

In this chapter we will present investigations aimed at the formation and the properties of the $(CO)_2^+$ ion (or more appropriately the $C_2O_2^+$ ion). Particularly the neutral $(CO)_2$, from which the experiment starts, will be termed a dimer, since it only contains one van der Waals bond. In analogy an $Ar(CO)_2$ cluster will be termed trimer.

The properties of neutral $(CO)_2$ have recently been investigated by microwave spectroscopy by Vanden Bout et al. [139], and Havenith et al. [140]. Both a planar T shape [139] and a non-planar crossed conformation [140] have been discussed as possible equilibrium structures. However, the question remains whether it is appropriate to think in terms of one equilibrium structure, since the potential energy surface is extremely flat [141,142] exhibiting several energy minima and saddle points within a range of about 12 meV. The calculated binding energy of the neutral $(CO)_2$ is $D_e = 18$ meV.

It may be useful to point at another molecule with the sum formula C_2O_2, the elusive carbon suboxide (ethylenedione). Theory predicts that the linear $^3\sum_g^-$ ground state should be stable with respect to spin allowed dissociation [143]. But despite considerable effort dating back to the beginning of the last century [144] it has not been detected experimentally beyond doubt. Possible reasons have been disputed extensively in the literature [143,145,146]. Most recently Schröder et al. [147] demonstrated that ethylenedione is an intrinsically short lived molecule due to a spin–orbit-induced coupling to an unbound electronic state. This ethylenedione must not be confused with the $(CO)_2$ van der Waals dimer present in a neutral CO cluster beam.

The $(CO)_2^+$ ion was first studied in a high pressure mass spectrometric (HPMS) investigation [148]. Employing electron impact ionization an appearance energy of 12.8 ± 0.3 eV was derived. Combining this with the IE of the CO molecule (14.014 eV [69]), one arrives at a binding energy of the $(CO)_2^+$ ion of 1.2 ± 0.3 eV with respect to Eq. (21)

$$(CO)_2^+ \rightarrow CO^+ + CO \quad (21)$$

In later work the reaction enthalpy was measured directly as $-\Delta H > 24.5$ kcal/mol (>1.06 eV) [149]. The investigation of the reverse reaction, i.e., reaction Eq. (22) leads to binding energies of the $(CO)_2^+$ ion consistent with the results already mentioned. In a study of Eq. (22) employing rotationally state-selected CO^+ ions Gerlich and Rox [150] found that the rate constant for association only depends on the total energy, irrespective of whether it has been put into translation or rotation.

$$CO^+ + 2\,CO \rightarrow (CO)_2^+ + CO \quad (22)$$

From electron impact ionization of CO cluster beams the AE of $(CO)_2^+$ was derived as 13.19 ± 0.1 eV [151,152]. The photoionization of CO clusters was first investigated by Linn et al. [153]. From the photoion yield curve they derived an AE of the $(CO)_2^+$ ion of 13.05 ± 0.04 eV. By the same technique Ding et al. [154] derived a value of 13.15 eV. Interestingly the same value was also obtained for the ions $(CO)_3^+$ and $Ar(CO)_2^+$. In an experiment looking at energy-selected carbon monoxide cluster ions Norwood et al. determined the IE of $(CO)_2$ as 12.73 ± 0.05 eV [155,156]. Most likely this is still an upper bound since possible contributions from dissociative ionization of larger clusters were not taken into account. Again combining this number with the IE of the monomer CO (14.014 eV) and the binding energy of the neutral $(CO)_2$ of 18 meV [141] one obtains a binding energy of the $(CO)_2^+$ ion corresponding to Eq. (21) of 1.30 ± 0.05 eV [156]. In a SIFT study [157] the heat of reaction for Eq. (21) was also determined as 1.1–1.3 eV. While obviously most of the published work points at a binding energy of $(CO)_2^+$ of about 1.2 eV, a significantly higher value was reported by Chen and Holmes [146]. There the AE of the $(CO)_2^+$ ion was determined by dissociative ionization of various precursors, e.g., quadratic acid. From that the binding energy of $(CO)_2^+$ was derived as >1.96 eV. If this value were correct this would be the strongest bond in an ionized van der Waals cluster. Here, the question first arises, whether the formula $(CO)_2^+$ is a good representation of the binding situation in this system.

The first ab initio calculations of the $(CO)_2^+$ ion was reported by Beebe and Sabin [158]. Knight et al. [159] described CI calculations of a non-linear *trans*-bent ^2B_u ground state of this ion. Blair et al. [160] calculated the ground and the excited state of the $(CO)_2^+$ ion. At the MP2/6-31G* level again a *trans*-planar equilibrium geometry was found for the ground state. The C–C bond length was only 1.505 Å

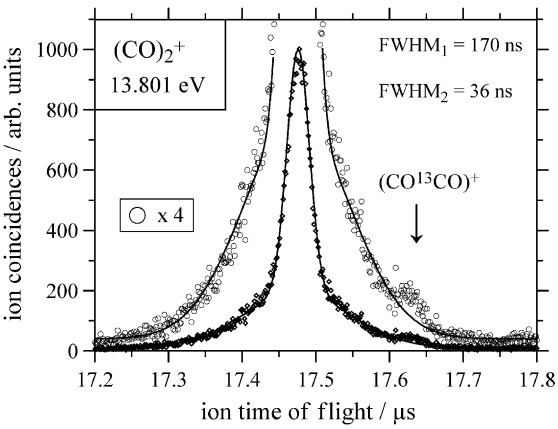

Fig. 12. TPEPICO-TOF spectrum of the $(CO)_2^+$ ion at 13.801 eV. Symbols: experimental data; lines: simulation employing two Gaussians [162]. Part of the spectrum is also enlarged (4×).

and the C–C–O bond angle 144.3°. The two C–O bond length were fixed at 1.13 Å, which is very similar to that of the neutral isolated C–O molecule. The binding energy of the $(CO)_2^+$ ion was calculated to be $D_e = 2.68$ eV. Since vibrational frequencies were not reported, we cannot convert this to D_0. A C_{2h} symmetry was also observed in a Neon matrix by IR spectroscopy [161].

In an attempt to settle this controversy on the binding energy of the $(CO)_2^+$ ion we have investigated the formation of $(CO)_2^+$ ions in a carbon monoxide cluster beam seeded in argon. Experimental details are given in [162]. Fig. 12 presents a TPEPICO-TOF spectra of the $(CO)_2^+$ ion recorded at 13.801 eV. The spectrum exhibits a narrow and a broad component. Thus, the experimental data were again simulated by the sum of two Gaussians, whose FWHM is indicated. For data obtained in a range from 13.4 to 14.0 eV the FWHM of the two components was translated to the kinetic energy of the $(CO)_2^+$ ions by employing Eqs. (5)–(7). The narrow component here corresponds to a translational temperature of 27 K, corresponding to the transversal translational temperature of the cluster beam. This narrow component is due to the non-dissociative ionization of neutral $(CO)_2$. The broad component is again caused by dissociative ionization. Over the range of accessible excitation energies (13.5–14.0 eV) the FWHM of the broad component was found to increase from 150 to 180 ns. This corresponds to a kinetic energy released into the $(CO)_2^+$ ion (KER[$(CO)_2^+$]) of 73–107 meV. Here, we assumed that the translationally hot $(CO)_2^+$ ions were formed by dissociative ionization of $Ar(CO)_2$ clusters as indicated in Eq. (23).

$$\begin{aligned} Ar(CO)_2 + h\nu &\rightarrow Ar(CO)_2^+ + e^- \\ &\rightarrow (CO)_2^+ + Ar + e^- \end{aligned} \quad (23)$$

As a next step we compare these experimental KER data with the KER expected from theory. For an application of Eq. (9) we again need the vibrational frequencies of the $(CO)_2^+$ ion. At the time of this investigation these frequencies were not available in the literature which motivated us to perform high level ab initio calculations ourselves.

The starting point for our calculations was the equilibrium geometry of the $(CO)_2^+$ ion reported by Blair et al. [160]. The latter corresponds to local minimum since not all geometry parameters had been optimized. Full geometry optimization at the MP2/6-31G* level, which was also employed by Blair et al. led to a global minimum with *trans*-planar geometry. The equilibrium length of the C–C bond is 1.459 Å, which is closer to that in neutral ethylenedione (1.281 Å [143]) than to the neutral $(CO)_2$ cluster (3.5 Å [141]). The vibrational mode analysis, however, yielded results which were quite surprising. For the asymmetric C–O stretching vibration a frequency of 7601 cm^{-1} was obtained, which can hardly be considered to be realistic. Interestingly this extremely high frequency was not observed at the UHF level [162]. However, the UHF values calculated for the symmetric and asymmetric stretch vibration of about 2480 cm^{-1} are still significantly larger than in the isolated neutral CO (2146 cm^{-1} [163]) and in the CO^+ ion (2194 cm^{-1} [161]), as well as those experimentally observed in the $(CO)_2^+$ ion [161]. Self-consistent results were only obtained when going to the QCISD/6-311G* level at which we were able to perform geometry optimization and frequency calculations. There the C–C bond length is 1.601 Å, which is certainly

shorter than expected for a van der Waals bond. The C–O bond lengths are 1.133 Å, and the bond angle is ∡ O–C–C is 141.5°. Our calculations confirm that the $(CO)_2^+$ ion is *trans*-planar. The asymmetric and the symmetric stretching vibration have frequencies of 2087–2120 cm^{-1}. The absolute value of these two frequencies as well as their difference agrees very well (deviation $< 50\,cm^{-1}$) with the combined IR spectroscopic and theoretical study of Thompson and Jacox [161]. There are also four low frequency vibrations (168, 185, 328, 579 cm^{-1}). A population analysis revealed that the charge as well as the spin population are localized on the two central C atoms.

Based on the vibrational frequencies of the $(CO)_2^+$ ion described one is able to calculate the theoretically expected KER[$(CO)_2^+$] assuming that the translationally warm $(CO)_2^+$ are formed by statistical dissociation of intermediary $Ar(CO)_2^+$ ions according to Eq. (23). Here we employ the original Klot's equation (Eq. (23)) with $r = 3$ since the $(CO)_2^+$ ion is non-linear. In order to compare that fraction of the total experimental KER which is observable in the $(CO)_2^+$ ion ($KER[(CO)_2^+] = KER_{tot} \times M_N/M_P$) with the theoretical KER in one diagram, one has to assume an AE for reaction Eq. (23). The best agreement between experimental and theoretical data is obtained for a value of $AE = 12.25 \pm 0.15$ eV (see Fig. 13). The adiabatic ionization energy is connected with this AE through Eq. (24).

$$AE = [(CO)_2^+] = IE[(CO)_2] + BE[Ar(CO)_2] \quad (24)$$

Assuming that the binding energy in neutral $Ar(CO)_2$ is 14 meV—similar to that in neutral ArCO [164], we arrive at an adiabatic IE of the neutral CO dimer of 12.24 ± 0.15 eV and for the binding energy of the $(CO)_2^+$ ion of 1.80 ± 0.15 eV. From this we derived a new picture of the energetics in argon/carbon monoxide clusters as depicted in Fig. 14. Strictly the binding energies of the neutral clusters indicated in Fig. 14 correspond to D_e values. A transformation to D_0 values would only be possible if the normal modes of that cluster were known, which is not the case. However, the error introduced by this is supposed to be small compared to the energy resolution of the experiment (about 20 meV).

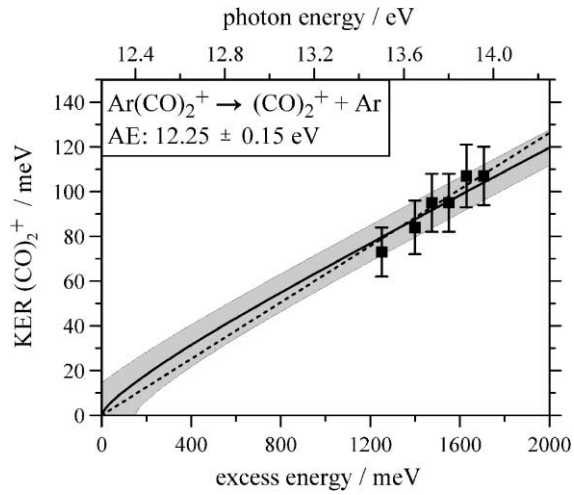

Fig. 13. Average KER[$(CO)_2^+$] based on the reaction indicated. Symbols: experimental data; solid line: Klots equation; dashed line: modified Franklin equation. The shaded area indicates the estimated uncertainty [162].

In addition we have calculated the binding energy of the $C_2O_2^+$ at the QCISD/6-311G* level to be 1.98 eV [162]. Our experimental as well as our ab initio result are fully compatible with the recent study of Chen and Holmes [146], but significantly larger than all other experimental studies. The following reasons might explain this discrepancy. The other PI studies probably determined the vertical threshold for dissociative ionization and thus only an upper limit to the IE. In the SIFDT experiment the system possibly did not reach equilibrium. The very high ab initio value of Blair et al. [160] is most likely caused by short comings of the MP theory which also causes an extremely high stretching frequency. The binding energy of the $(CO)_2^+$ ion of 1.80 eV is certainly one of the largest ever observed for an ionized van der Waals cluster. In fact all the information available suggests that we are dealing with a molecular ion rather than a cluster ion. This ion is in fact the ethylenedione ion, $C_2O_2^+$, which is here only formed by a chemical reaction within a van der Waals cluster.

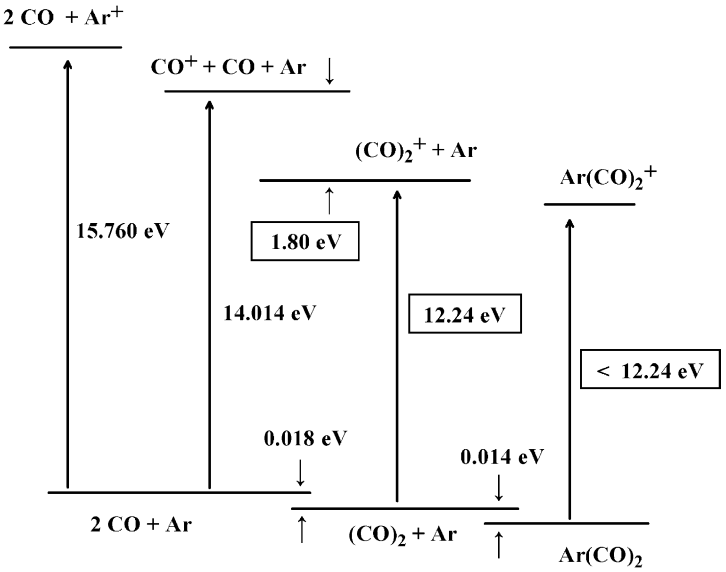

Fig. 14. Energetics of the argon/carbon monoxide cluster system with respect to $(CO)_2^+$ ions. Values from our work [162] are marked by a box. The other data are from the literature [69,141,164].

4.3. Nitrogen cluster: the formation of $(N_2)_2^+$

In this chapter we will discuss experiments aimed at the dissociative formation of $(N_2)_2^+$ ion, which is isoelectronic to the $(CO)_2^+$ ion discussed in the previous chapter. The question is whether these two systems do in fact have similar geometry, binding energy, etc.

$$(N_2)_2^+ \rightarrow N_2^+ + N_2 \quad (25)$$

In an early high pressure mass spectrometry (HPMS) study Munson et al. [148] the appearance energy of the $(N_2)_2^+$ ion was determined to be 14.3 eV, which combined with the IE of N_2 leads to a binding energy of the $(N_2)_2^+$ ion with respect to the dissociation into two nitrogen molecules (Eq. (25)) of about 1.3 eV. From gas phase equilibrium studies the enthalpy of the reaction $N_2^+ + 2\,N_2 \rightleftharpoons (N_2)_2^+ + N_2$ was derived as 22.8 kcal/mol (0.99 eV) [165], 24.4 ± 2.1 kcal/mol (1.06 ± 0.09 eV) [166], and 25.8 ± 1.5 kcal/mol (1.12 ± 0.07 eV) [167]. The binding energy of the $(N_2)_2^+$ ion according to Eq. (25) has been obtained from photoion yield spectra [153] and electron impact ionization [168] of nitrogen cluster beams as 0.9 ± 0.05 and 0.9 ± 0.2 eV, respectively. From PEPICO experiments, Norwood et al. [169] derived an adiabatic IE of neutral $(N_2)_2$ of 14.5 ± 0.08 eV corresponding to a binding energy of $(N_2)_2^+$ of 1.09 ± 0.08 eV. The same value was also obtained from a collision-induced dissociation (CID) experiment (1.09 ± 0.06 eV) [170]. Lindinger et al. [200] performed drift tube experiments over a very wide range of effective temperatures. From the Arrhenius behavior observed over 56 decades a binding energy of the $(N_2)_2^+$ ion of 0.83 ± 0.05 eV was derived. Early ab initio SCF calculations predicted a binding energy of $D_0 = 1.32$ eV [171]. A valence bond study reported a value $D_e = 1.127$ eV [172]. A very recent coupled-cluster calculations reported a value of $D_0 = 1.21$ eV ($D_e = 1.26$ eV) [173]. In a matrix, the equilibrium geometry of the $(N_2)_2^+$ ions has been shown to be linear [174]. Additional ab initio calculations revealed that the spin density is mainly located at the two central (N) atoms, similar to the $(CO)_2^+$ ion. Thus, the literature values reported for the binding energy of the $(N_2)_2^+$ ion are similar to most of the older values for the $(CO)_2^+$ ion. The latter, however, turned out to be too small. The question arises whether $(N_2)_2^+$ and $(CO)_2^+$ really have

similar binding energies or not. It is interesting to note that the equilibrium geometry of the $(N_2)_2^+$ ion is linear while that of the $(CO)_2^+$ ion is *trans*-bent.

Here, we report for the first time the investigation of the $(N_2)_2^+$ ion by the translational energy spectroscopy employed for the Ar_2^+ and $(CO)_2^+$. In this experiment a mixture of argon and nitrogen (pressure ratio 1:5) was expanded through a 50 μm nozzle operated at 170 K. The electric field was 20 V/cm, the overall resolution 20 meV. The TPEPICO-TOF spectra of this cluster beam were studied in the range from 15.15 to 15.35 eV.

A high resolution TPEPICO-TOF spectrum of the $(N_2)_2^+$ ion is presented in Fig. 15. Again one clearly sees one narrow component, due to the non-dissociative ionization of neutral $(N_2)_2$ clusters, and one broad component, due to the dissociative ionization of a larger cluster. In general the energy range accessible by our experiment is limited by low Franck–Condon factors on the low energy side and by the IE of the monomers on the high energy side. Unfortunately this leads to a very small energy range in this system. However, we will show that nevertheless valuable information can be derived.

The average kinetic energy released into the $(N_2)_2^+$ ion was deduced from the FWHM of these TOF spectra. In analogy to the other systems discussed in this work we again assumed that an argon atom is evaporated in the dissociative ionization as indicated in

$$Ar(N_2)_2 \rightarrow Ar + (N_2)_2^+ \quad (26)$$

This implies the formation of an intermediate $Ar(N_2)_2^+$ ion. In a recent plasma study a centrosymmetric linear structure of the $Ar(N_2)_2^+$ has been observed [175]. However, other isomers may exist and it is not clear which of the neutral isomers dominates the current experiment. The average KER[$(N_2)_2^+$] from the current work is plotted in Fig. 16 as a function of the photon energy. Because of the limited energy range, we did not perform high level statistical calculations for the KER so far. In order to allow for a first estimate of the adiabatic IE of $(N_2)_2$ and the binding energy of $(N_2)_2^+$, respectively, we have performed a modified Franklin calculation (Eq. (20)). We have to emphasize again, that the scaling factor 0.6 in Eq. (20) was tested against the other cluster systems studied and found to yield reliable results.

As shown in Fig. 16 this calculated KER[$(N_2)_2^+$] agrees with the experimental KER if we assume a threshold for the dissociative ionization of $Ar(N_2)_2$ clusters of 14.55 eV. Assuming further that the binding energy of a neutral $Ar(N_2)_2$ cluster is about 14 meV,

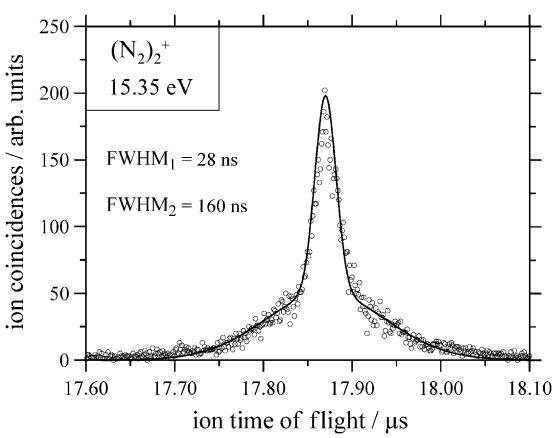

Fig. 15. TPEPICO-TOF spectrum of the $(N_2)_2^+$ ion recorded in an argon/nitrogen cluster beam at 15.35 eV.

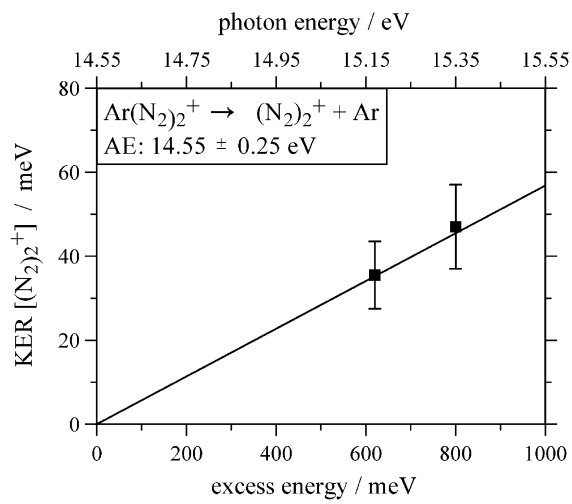

Fig. 16. Average KER[$(N_2)_2^+$] based on the reaction indicated. Symbols: experimental data; lines: modified Franklin calculation (Eq. (20)).

similar to that in mixed Ar/CO clusters (see next chapter), we arrive at an adiabatic IE of $(N_2)_2$ of 14.54 ± 0.25 eV and a binding energy of the $(N_2)_2^+$ ion of 1.06 ± 0.25 eV. This value is in agreement with the information in the literature. Thus, the binding energy of the $(N_2)_2^+$ ion is significantly smaller than that of the isoelectronic $(CO)_2^+$ ion (1.8 eV). This once more confirms the uniqueness of the $(CO)_2^+$ ion. While the latter is in fact a molecular ion with high binding energy, a similar stabilization does not exist for the $(N_2)_2^+$ ion.

4.4. Argon/carbon monoxide cluster: the formation of $ArCO^+$

In the previous chapters we have discussed the properties of homogeneous argon, nitrogen and carbon monoxide dimer ions (although the $C_2O_2^+$ turned out to be a molecule rather than a dimer). To complement the study of these systems we will now turn to the mixed clusters. More specifically we have been able to study the properties of $ArCO^+$ and ArN_2^+. Mixtures of nitrogen and carbon monoxide have not been investigated since these two molecules have identical mass ($m/z = 28$). In the next chapter we will first describe the $ArCO^+$ ion. Again we use the term dimer for this system since it contains only one van der Waals bond.

From numerous theoretical [176–183] and experimental [184–190] studies the neutral ArCO dimer is known to have a triangular equilibrium geometry, in which the CO bond length is similar to that of the isolated molecule (about 1.13 Å) and the distance between the argon atom and the CO center of mass is about 3.6–4 Å. There are two extremely low frequency modes in the ArCO, one stretching vibration of $18\,cm^{-1}$ [183,187] and one bending vibration of about $12\,cm^{-1}$ [183,187]. Nevertheless, the internal rotation of the CO unit does not seem to be free [191] (at least for the rotational ground state). The CO stretching vibration in ArCO is observed at $2143\,cm^{-1}$ [185] almost identical to that of the isolated CO molecule. The binding energy of ArCO with respect to dissociation (D_e) into Ar and CO has been calculated to be in the range of 8–20 meV [176,177,179,191]. From the frequencies discussed the difference between D_e and D_0 should be on the order of 2 meV, and thus negligible.

The appearance energy of the $ArCO^+$ ion was determined by HPMS [148] with 14.2 eV. From photoion yield measurements in an argon/carbon monoxide cluster beam Ding et al. derived an AE of 13.4 eV [154]. The same value was also obtained for the next larger cluster ion Ar_2CO^+. Norwood et al. [192] performed the first TPEPICO experiments in an Ar/CO cluster beam and reported an AE of 13.33 eV. Combining this AE with the IE of the CO monomer of 14.014 ± 0.06 eV [69] and the binding energy D_0 of neutral ArCO (about 12 meV), one arrives at a binding energy of the $ArCO^+$ ion of 0.70 eV. In theoretical work values of 0.93 eV [193] and 0.68 eV [194] were reported for D_e. The latter work assumed a linear equilibrium geometry of the $ArCO^+$ ion (Ar–C–O). The geometry of neutral or ionic $Ar_2(CO)$ clusters was not known previously.

In order to shed new light on the equilibrium geometry and the energetics of the $ArCO^+$ ion we have investigated the dissociative formation of $ArCO^+$ ions in the photoionization of an Ar/CO cluster beam in a TPEPICO experiment [43]. These experiments were performed under conditions identical to the ones applied for the $C_2O_2^+$. A typical TPEPICO-TOF spectra of the $ArCO^+$ ion recorded at 13.801 is shown in Fig. 17. The TOF distribution in Fig. 17 clearly exhibits a narrow and broad contribution which can be simulated by Gaussian functions. Again the FWHM of the narrow component (34 ns) is independent of the photon energy, indicating that these ions are formed by non-dissociative ionization of ArCO. This width translates to about 3 meV (Eq. (5)) which corresponds to a translational temperature of 25 K.

The broad component is due to the dissociative ionization of a larger cluster which is accompanied by KER. Employing Eq. (7) the width of this component allows to derive the average KER released into the $ArCO^+$ ion assuming that this component is caused by reaction Eq. (27), i.e., from an Ar_2CO parent cluster.

$$\begin{aligned} Ar_2CO + h\nu &\rightarrow Ar_2CO^+ + e^- \\ &\rightarrow ArCO^+ + Ar + e^- \end{aligned} \quad (27)$$

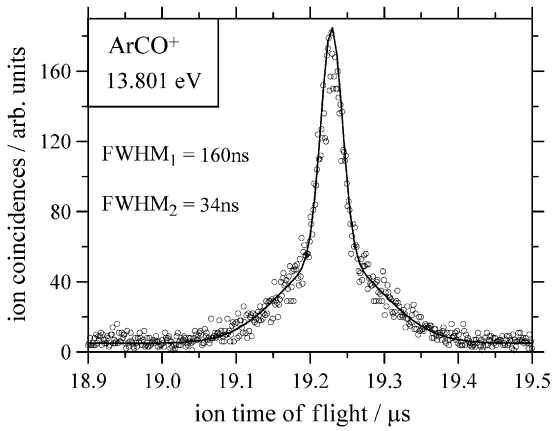

Fig. 17. TPEPICO-TOF spectrum of the $ArCO^+$ ion, recorded at 13.801 eV. Symbols: experimental data; line: simulation by sum of two Gaussians [52].

In order to be able to compare experimental KER information with theoretical data and consequently determine adiabatic threshold energies by extrapolation to KER = 0 we again need ab initio information on the equilibrium geometry (linear or non-linear?) and vibrational frequencies of the $ArCO^+$ ion. In two previous reports [193,194] the $ArCO^+$ was assumed to be linear (in analogy to the ArN_2^+ ion, see next chapter). The vibrational frequencies had not been reported previously. In our own ab initio calculations [195] we found a non-linear equilibrium geometry at all levels of computation employed. This is in fundamental contrast to all previous assumptions. The energy difference between a frozen linear and the optimized non-linear geometry is, however, only on the order of 25 meV, i.e., relatively small. The non-linear $ArCO^+$ ion has only three vibrational degrees of freedom, but also three rotational degrees of freedom (linear $ArCO^+$: 4/2) which is crucial for the statistical calculations of the KER. At the QCISD/6-311G(2df) level the C–O bond length is 1.116 Å, the Ar–C bond length is 2.225 Å, and the bond angle ∡ Ar–C–O is 149.6°. According to a Mulliken population analysis the charge density is basically delocalized over the terminal argon and the central carbon atom. A NBO analysis yields for the natural charge at the argon, carbon and oxygen, values of 0.37, 0.87 and −0.24, respectively.

Based on the geometry parameters and the vibrational frequencies [195] of the $ArCO^+$ one can calculate the average KER in the formation of the $ArCO^+$ ion by numerical solution of Eq. (9). The use of the original Klots equation seems appropriate in this case since the Ar_2CO^+ ion has a non-linear equilibrium conformation according to our QCISD/6-311G(2df) calculation. Assuming that the translationally warm $ArCO^+$ ions are formed by the process given in Eq. (27), i.e., the dissociative ionization of neutral Ar_2CO, one can derive the average KER($ArCO^+$) observable in the $ArCO^+$ ion. This is plotted in Fig. 18 together with the experimental KER($ArCO^+$). In addition Fig. 18 shows the average KER($ArCO^+$) calculated from PST (for parameters see the Appendix A). The latter calculation was based on rotational constants of the Ar_2CO^+ ion calculated at the QCISD/6-311G* level. Details of this analysis are presented elsewhere [52]. At this point we wish to emphasize that the results of Klots and PST calculations are almost identical. Best agreement between experimental and theoretical KER($ArCO^+$) is obtained for a threshold energy of AE = 13.04 eV for the formation of $ArCO^+$ ions from neutral Ar_2CO clusters. Combining this AE with the binding energy

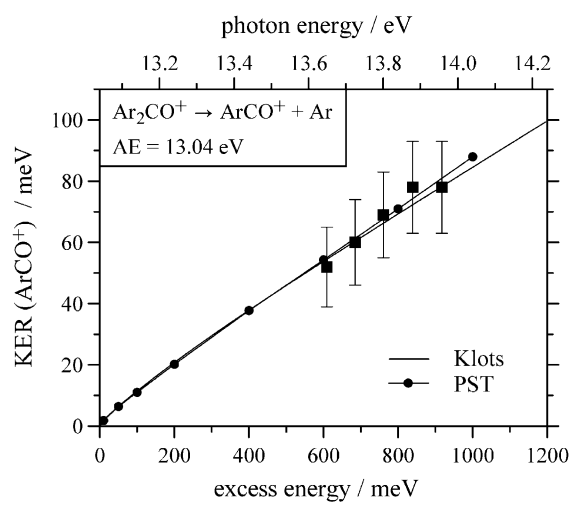

Fig. 18. Average KER($ArCO^+$). Symbols (■): experimental data as function of photon energy; lines: calculated KER($ArCO^+$) as function of the excess energy [52].

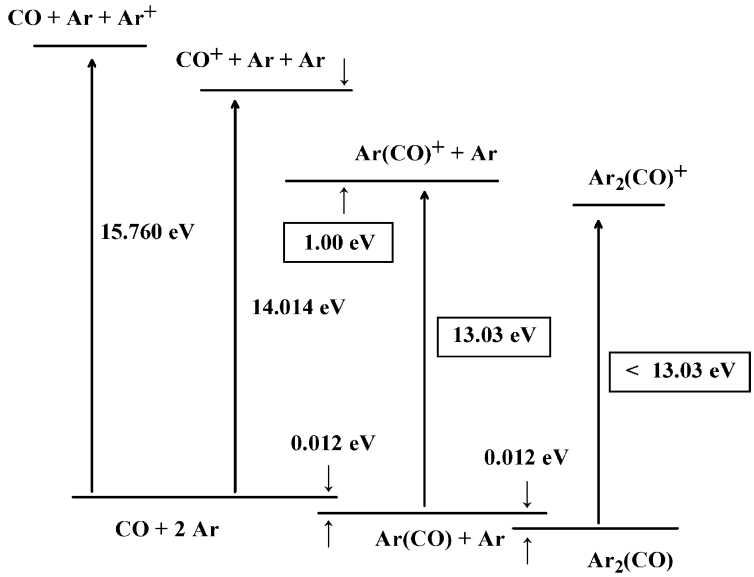

Fig. 19. Energetics of the argon/carbon monoxide system [69,180]. Information from the authors work marked by box.

of neutral Ar_2CO clusters according to Eq. (28) the adiabatic IE of neutral ArCO can thus be derived.

$$IE(ArCO) = AE(ArCO^+) + BE(Ar_2CO) \quad (28)$$

Assuming a value of 12 meV [180] for the binding energy of Ar_2CO, similar to that in neutral ArCO, we thus arrive at an adiabatic ionization energy of IE = 13.03 ± 0.15 eV. Combining this result with the established IEs of the monomers [69], one arrives at the picture of the energetics of the argon/carbon monoxide cluster system referenced to Ar_nCO clusters as shown in Fig. 19. For a comparison see also the energetics for the $Ar(CO)_2$ cluster (Fig. 14). Finally, this analysis led to a new value for the binding energy of the $ArCO^+$ ion with respect to $Ar + CO^+$ of $BE(ArCO^+) = 1.00 \pm 0.15$ eV. This value is compatible the value of 0.93 eV reported by Hamilton et al. [193]. However, it is significantly higher than all experimental values reported previously and also higher than the theoretical value reported by Archirel [194]. We have also calculated the dissociation energy of the $ArCO^+$ ion by means of ab initio calculations. At the CCSD(T)/aug-cc-pVTZ level we obtained a value of $D_0 = 0.94$ eV and with the CBS-Q approach $D_0 = 0.98$ eV in nice agreement with the experimental value.

The KERDs of the PST calculations, from which the average KER discussed above had been derived, are very similar to those calculated for the Ar_2^+, i.e., the most probable KER is always KER = 0. Despite this similarity the probability for observing products with one particular excess energy shows a different correlation with the rotational angular momentum of the parent. This flux into the $ArCO^+$ product ion is shown in Fig. 20. For small KER again much of the flux has to go through high *J* states. We note, however, that here the contribution of low *J* states is significantly larger than in the Ar_2^+ case. Most likely this reflects the difference in the equilibrium geometry of the two product ions (linear Ar_2^+ vs. non-linear $ArCO^+$).

4.5. Argon/nitrogen cluster: the formation of ArN_2^+

This chapter describes the formation of ArN_2^+ ions by dissociative ionization of mixed argon/nitrogen clusters. In the current context the ArN_2^+ ion is particularly interesting since it is isoelectronic with the $ArCO^+$ ion discussed above. For the $(N_2)_2^+$ and the

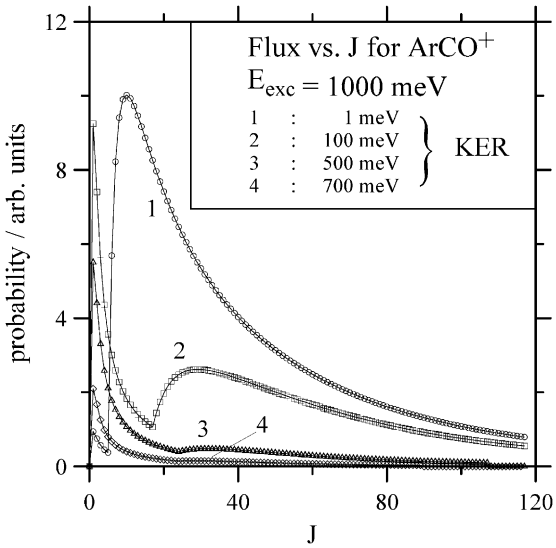

Fig. 20. Probability for observing $ArCO^+$ with a specific kinetic energy release KER as a function of the rotational angular momentum J of the Ar_2CO cluster ($E_{exc} = 1000$ meV).

$(CO)_2{}^+$, which are also isoelectronic, we found different equilibrium geometries and different binding energies. Now, we approach the question, whether $ArN_2{}^+$ and $ArCO^+$ have similar equilibrium geometries and binding energies.

Early work by Kaul and Fuchs [196] reported the formation of $ArN_2{}^+$ ions in the electron impact ionization of argon/nitrogen mixtures. By variation of the electron energy an appearance energy of 15.1 ± 0.5 eV was derived. By means of HPMS Munson et al. [148] obtained an AE for the $ArN_2{}^+$ ion of 14.6 ± 0.2 eV. By combination with the IE of the nitrogen molecule (15.581 eV) [69] this would lead to a binding energy of the $ArN_2{}^+$ ion according to Eq. (29) of $D_0 = 0.98$ eV. In SIFT experiments the dissociation energy of $ArN_2{}^+$ was found to be 0.91 eV [157].

$$ArN_2{}^+ \rightarrow Ar + N_2{}^+ \tag{29}$$

From equilibrium studies of various ion–molecule reactions Teng and Conway [166] derived a binding energy (extrapolated to 0 K) of 1.14 ± 0.1 eV. Hiraoka et al. arrived at a value of 1.16 eV by a similar technique [197]. Stimulated by the similarity of the ionization energy of argon and nitrogen the charge transfer reaction (Eq. (30)) received extensive interest and the rate constants were determined as a function of the translational energy or of the internal energy of the nitrogen (either in forward or backward direction) [198–203].

$$Ar^+(^2P_{3/2}, {}^2P_{1/2}) + N_2 \rightarrow N_2{}^+ + Ar \tag{30}$$

This charge transfer process has also been the subject of theoretical studies [204,205]. Additional information on the $ArN_2{}^+$ ion can be derived from investigations of the ion molecule reactions between $(N_2)_2{}^+$ ions and Ar leading to $ArN_2{}^+$ and N_2 [166,206,207], which appears to be thermoneutral. Extensive studies dealt with the photodissociation of argon/nitrogen cluster ions [208,209]. From the KER analysis of the products in the laser photolysis of $ArN_2{}^+$ ions Kim and Bowers [206] concluded that this ion is linear in its ground state. Stephan and Märk [210] observed the metastable decay of $ArN_2{}^+$ ions in the electron impact ionization of cluster beams. This was not confirmed by work of Illies and Bowers [211]. From a CID study of the $(N_2)_2^+$ + rare gas system a binding energy of the $ArN_2{}^+$ was tentatively derived as 1.05 ± 0.07 eV [170]. The photoionization of argon/nitrogen clusters was investigated by Ding et al. [154]. The ion yield curves observed show a very shallow increase in the threshold region, which makes the unambiguous determination of ionization energies difficult. The AE of $ArN_2{}^+$ and $Ar_2N_2{}^+$ were reported as 14.7 and 14.5 eV, respectively. The photodissociation of $Ar_2N_2{}^+$ at 532 nm [209,212] leads to only Ar^+, $Ar_2{}^+$ and $N_2{}^+$, but no $ArN_2{}^+$.

Only few theoretical calculations of argon/nitrogen clusters are known. The binding energy of ArN_2, relative to Ar + N_2, was calculated as 13.9 meV [213]. The equilibrium geometry is triangular. Several groups reported UHF ab initio calculations indicating a linear equilibrium conformation of the $ArN_2{}^+$ ions [214,215]. Hiraoka et al. [215] confirmed the linear structure by MP2 geometry optimizations, however, no normal coordinate analysis was reported at that level. The $Ar_2N_2{}^+$ is believed to have a linear equilibrium geometry [216]. While only one structural

isomer exists for the ArN_2^+ ion ($N_{terminal}$–$N_{central}$–Ar) at least two isomers exist for the $Ar_2N_2^+$ ion, corresponding to the Ar–N–N–Ar^+ and Ar–Ar–N–N^+ structure. Both isomers are linear, with the latter being more stable by about 21 meV [215]. Most likely several isomers also exist for the neutral Ar_2N_2 in a cluster beam.

We have also investigated the energetics of the argon/nitrogen cluster ions by means of the TPEPICO technique [217]. A high resolution TPEPICO-TOF spectrum of the ArN_2^+ ion recorded at 15.549 eV is shown in Fig. 21. The narrow component of the signal again corresponds to the non-dissociative ionization of neutral ArN_2 correlating with the translational temperature of the cluster beam, while the broad component corresponds to translationally warm ArN_2^+ ions formed by dissociative ionization of a larger cluster. Experimental details of this work are given in [217].

In the range of photon energies available the width of the broad component varies from 100–180 ns. The uncertainty in the FWHM is typically ±15 ns. Assuming that reaction in Eq. (31) is responsible for the dissociative formation of ArN_2^+ ions this translates to an average KER(ArN_2^+) of 27–89 meV.

$$Ar_2N_2 + h\nu \rightarrow Ar_2N_2^+ + e^- \rightarrow ArN_2^+ + Ar + e^- \quad (31)$$

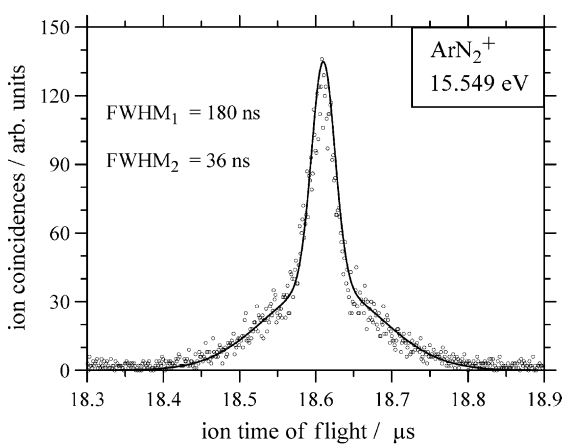

Fig. 21. TPEPICO-TOF spectrum of the ArN_2^+ ion recorded at 15.549 eV (symbols: experimental data; line: simulation) [217].

The calculation of the KER(ArN_2^+) expected based on a statistical dissociation of $Ar_2N_2^+$ ions requires some knowledge of the relevant structures and vibrational frequencies. Here the attempt to calculate vibrational frequencies at the geometry reported by Hiraoka at el. [215] showed, that this was only a saddle point at that level of computation. This stimulated extensive ab initio calculations on our side, which finally confirmed the linear equilibrium geometry of the ArN_2^+ ion [217]. The important result of that investigation is that the MP2 calculations should be viewed with caution. Similar to, e.g., the $C_2O_2^+$ ion (see above) the MP2 calculations yield unreasonably high vibrational frequencies.

At the highest level employed (QCISD(FC)/6-311G*) the linear equilibrium geometry of the ArN_2^+ ion is clearly confirmed and the vibrational frequencies obtained (179, 179, 311, 2344 cm^{-1}) appear reasonable. Not even a local minimum is observed for a non-linear geometry. Single point calculations at the QCISD/6-311G* level show that the structure for which the global minimum was observed at the MP2/6-31G* level is more energetic by 0.2 eV compared to the linear structure. Mulliken and NBO population analysis based on the QCI density matrix show, that the charge density is mainly localized at the terminal argon atom. At this point it is clear that there are major differences between the properties of the ArN_2^+ ion and the isoelectronic $ArCO^+$ ion. For the ArN_2^+ ion the linear conformation turns out to be more stable, while for the $ArCO^+$ ion the non-linear conformation was more stable. This is also reflected in the difference in the charge distribution between the two ions.

Based on the ab initio results presented above we have calculated the KER(ArN_2^+) by different approaches. Originally we had employed Eq. (9), i.e., the original Klots equation [217]. As pointed out above this would be appropriate in the case of a non-linear parent cluster ion $Ar_2N_2^+$. Since neutral Ar_2N_2 is probably non-linear and vertical photoionization almost certainly leads to $Ar_2N_2^+$ ions with non-linear geometry. However, the calculations by Hiraoka as well as our own ab initio calculations suggest a linear

equilibrium geometry of the intermediate $Ar_2N_2^+$ ion. Our current understanding is that the theoretical KER analysis must be based on this linear geometry. Therefore, we have also calculated the KER(ArN_2^+) employing the modified Klots equation (Eq. (19)), where no rotational degree of the products is subtracted. Finally we have calculated the KER(ArN_2^+) employing PST (for parameters see the Appendix A). All these theoretical KER(ArN_2^+) curves are plotted in Fig. 22 as a function of the excess energy, while the experimental data are plotted as a function of the photon energy. Obviously the modified Klots and also the modified Franklin calculation agree very well with the experimental data—particularly with respect to the slope of the KER curve. Here the PST calculation predicts a slightly smaller slope which does not appear to represent the experimental data. Thus, the following analysis of the energetics will be based on the former. Possible reasons for the deviation of the PST calculation will be discussed below.

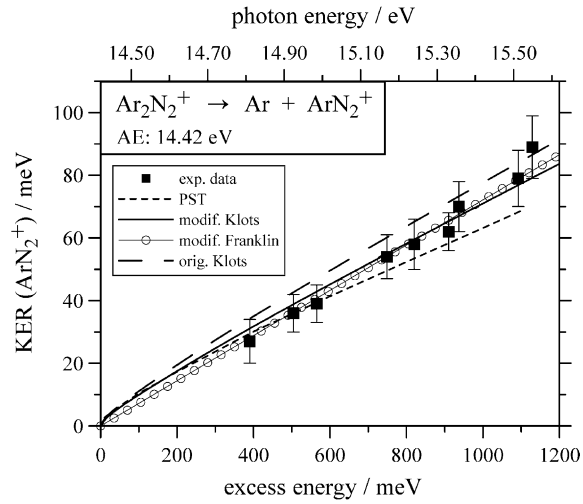

Fig. 22. Average KER(ArN_2^+). Symbols: experimental data; lines: calculated KER(ArN_2^+) based on the QCISD results and Eq. (29) [217] and Eq. (19).

Plotting the experimental and theoretical KER data mentioned above in one diagram requires the assumption of a threshold energy for the reaction given by Eq. (31). The best agreement between the modified Klots and Franklin calculations on one hand and the experimental data on the other is obtained for a threshold energy for the formation of ArN_2^+ of AE = 14.42 ± 0.10 eV. Employing Eq. (32) and

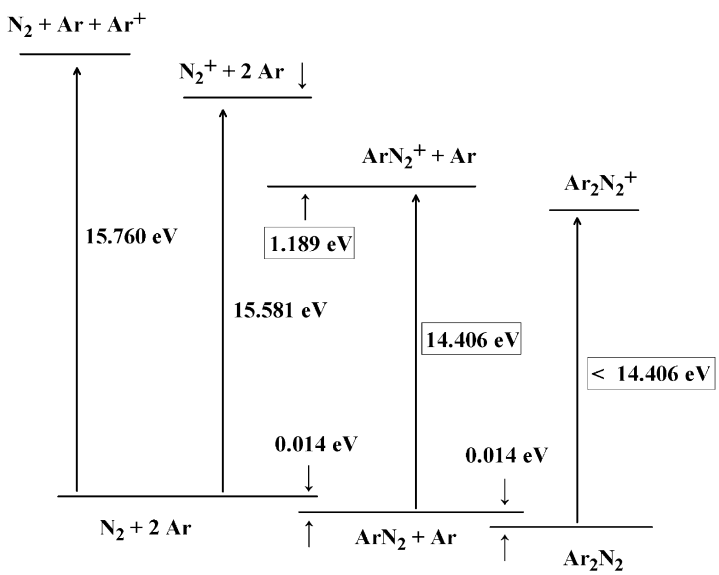

Fig. 23. Energetics of the argon/nitrogen system based on data from [69,213]. New results from this work are marked by a box.

assuming a binding energy of neutral Ar_2N_2 of 14 meV similar to that in ArN_2 [213], one arrives at an adiabatic IE(ArN_2) of 14.406 ± 0.10 eV.

$$AE(ArN_2^+) = IE(ArN_2) + BE(Ar_2N_2) \quad (32)$$

Combining these results with the IEs of the monomers and the estimated binding energy of the neutral clusters we derived a new picture of the energetics as shown in Fig. 23. Results derived in our lab are marked by a box. Besides from the IE(ArN_2) this is the dissociation energy of the ArN_2^+ with respect to Ar plus N_2^+ of 1.189 ± 0.10 eV. The latter is in reasonable agreement with most literature data. Our IE(ArN_2) is about 290 meV smaller than that derived by Ding et al. [154]. The pivotal point is, that we observe the formation of ArN_2^+ basically at the same photon energy as Ding et al. (about 14.7 eV), however, we see that these ArN_2^+ ions are translationally warm. Therefore, the true adiabatic threshold can only be lower than the actual photon energy.

As discussed above the average KER derived from the PST calculations showed a much smaller slope than both the experimental data and the two modified KER calculations, i.e., the KER appears to be too small at high excess energy. The complete KER distributions from which the average KER values are derived do not show any irregularities. They appear to be similar to those in the other systems where the PST has been applied. In an attempt to further analyze this discrepancy we have also investigated the effective flux into the ArN_2^+ product as a function of the parent rotational angular momentum. This flux is plotted in Fig. 24 for four different excess energies. For low excess energies the J dependence of the flux is similar to the one predicted for the formation of Ar_2^+. However, for large excess energies the contribution from the low J states appears smaller than expected. Since this flux is weighted by the parent rotational J distribution in the final calculation of the KERD, this may cause a low probability for large KER. Further analysis of these KERDs is required for a better understanding of the energy partitioning in the ArN_2^+ experiment.

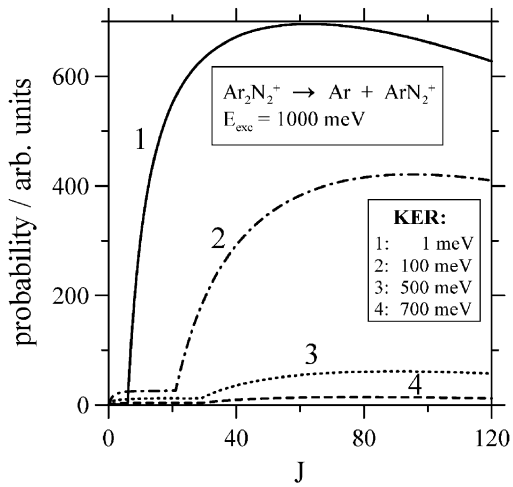

Fig. 24. Probability for observing ArN_2^+ with a specific kinetic energy release KER as a function of the rotational angular momentum J of the Ar_2N_2 cluster ($E_{exc} = 1000$ meV).

5. Summary and discussion

We have reviewed the thermochemistry of several small cluster systems with focus on the ionization energies and the ionic binding energies. Particular attention is given to work on the formation of three homogeneous cluster (dimer) ions (Ar_2^+, $(CO)_2^+$ and $(N_2)_2^+$) and two heterogeneous cluster (dimer) ions ($ArCO^+$ and ArN_2^+) performed in the authors laboratory. We have identified the contribution of dissociative and non-dissociative pathways in the photoionization of the corresponding neutral cluster beams and described a way to distinguish these contributions by means of TES. For the first time we have systematically investigated the KER of cluster ions in a TPEPICO experiment as a function of the excitation energy. By comparison with the theoretically expected KER and extrapolation to KER = 0, we have been able to determine the adiabatic IE of these clusters. This is very important since the direct ionization is not accessible at the adiabatic IE due to unfavorable Franck–Condon factors and significant geometry changes upon ionization.

The precursors of the dissociatively formed cluster ions are in general not observed in the coincidence

TOF spectra. This is due to the fact that a precursor cluster ion prepared with well defined internal energy above its dissociation threshold can and will in fact dissociate on the time scale of our experiment. The generalized conclusion from this is, that the absence of a certain cluster ion signal from a mass spectrum does not guarantee that the corresponding neutral was not present in the cluster beam. It only implies that there were no larger clusters in the beam. Indeed this is the recipe of our experimental approach: choose the expansion conditions such that dissociative ionization is barely observed but no ions from the corresponding precursors. This minimizes contributions from even larger clusters. Furthermore the conditions are chosen such that in all examples of this work a neutral argon atom is boiled off in the dissociative ionization.

Various approaches for estimating/calculating the KER expected were discussed. It turns out that the well known Klots's model is well suited for the dissociation of non-linear clusters. In general the KER must depend on the temperature of the cluster beam. This is not taken into account in the Klots model. In this respect the agreement with the more sophisticated PST presented in this work turns out to be accidental, i.e., only operative for the current temperature. The same holds true for the empirical Franklin equation, which is not capable of explaining any temperature dependence of the KER. In the case of a linear cluster ion significant differences between the original Klots model and PST were observed. These discrepancies, however, could be removed, by taking into account that the original Klots model only applies to non-linear molecules. This requires a different accounting of the rotational degrees of freedom of the system. In the PST, on the other hand, the geometry of all species involved is inherently taken into account.

The adiabatic IE of the clusters investigated in this work as well as the corresponding ionic binding energies are summarized in Table 1 and compared to experimental and theoretical literature data. For the Ar_2^+ ion our binding energy is between that of Norwood et al. [124] and Moseley et al. [121]. The binding energy derived for the $ArCO^+$ ion is slightly higher than most of the literature values. Our data agree reasonably well with the literature for the ArN_2^+ and the $(N_2)_2^+$ ion. Finally the binding energy derived for the $C_2O_2^+$ ion of about 1.8 eV is significantly higher than most literature reports, but agrees with a recent value from Chen and Holmes [146]. Good agreement between ab initio calculations and experiment as evident from Table 1 is only obtained at fairly high levels of computation requiring long cpu time. For a quick estimate of the thermochemistry complete basis set extrapolations (CBS) [218] represent an useful alternative. For the dimer ions listed in Table 1 ($Ar–Ar^+$, $CO–CO^+$, $N_2–N_2^+$, $Ar–CO^+$, and $Ar–N_2^+$) CBS calculations lead to binding energies of 1.37, 2.27, 1.33, 0.98, and 1.26 eV. Given the fact that these CBS calculations only require a few minutes of cpu time these results show surprising overlap with our experimental data.

As pointed out previously, the molecules CO and N_2 are isoelectronic. Thus, also the cluster ions $ArCO^+$ and ArN_2^+, respectively, $C_2O_2^+$ and $(N_2)_2^+$ are isoelectronic. While we found very similar binding energies for the $ArCO^+$ and the ArN_2^+ ion, the binding energies of the $C_2O_2^+$ and the $(N_2)_2^+$ ion differ by 0.7 eV. The ArN_2^+ ion has a linear equilibrium geometry, that of the $ArCO^+$ ion is non-linear. The Ar_3^+ ion is also linear. The $(N_2)_2^+$ ion is linear, while the $C_2O_2^+$ ion is bent (*trans*-planar). In the linear ArN_2^+ the charge is localized at the terminal argon atom. In the linear Ar_3^+ and in the non-linear $ArCO^+$ on the other hand, the charge is basically localized at the central argon, respectively, the central carbon atom. In both the $C_2O_2^+$ ion and the $(N_2)_2^+$ ion the charge is mainly localized at the central carbon, respectively, nitrogen atoms. Thus, there does not seem to exist a simple relation between the geometrical structure and the electronic structure. It may be worthwhile to point at yet another cluster ion isoelectronic with $C_2O_2^+$ and $(N_2)_2^+$, i.e., the $(N_2CO)^+$ ion. However, since the two constituent molecules CO and N_2 have almost identical mass, this system cannot be investigated in our experimental set-up.

One remarkable result of the current work is the binding energy of the $C_2O_2^+$ ion of 1.8 eV. This value makes it one of the largest binding energies of an ion derived from a neutral cluster. The pivotal

Table 1
Binding energies of small cluster ions determined in this work in comparison with literature

	$D_{0,exp.}$ (eV)	$D_{0,calc.}$ (eV)	Method	Reference
$Ar–Ar^+$		1.384	Morse	[106]
	1.33 ± 0.02		PD/TES	[121]
	1.32 ± 0.005		PI	[122]
		1.316	MRCI	[107]
	1.3147 ± 0.0008		PFI	[108]
	1.3130 ± 0.0007		PFI	[127]
	1.29 ± 0.05		PI/TES	This work
	1.27 ± 0.02		PI	[123]
	1.24		PI	[124]
$OC–CO^+$		2.68 (D_e)	MP2	[160]
		1.98	QCISD	This work
	1.96		Diss. EI	[146]
	1.80 ± 0.15		PI/TES	This work
	1.30 ± 0.05		PI	[155]
	1.1–1.3		SIFT	[157]
	0.99 ± 0.04		PI	[153]
	0.89		PI	[154]
	0.84		EI	[152]
$N_2–N_2^+$		1.21	CCSD	[173]
		1.127 (D_e)	VB	[172]
	1.12 ± 0.07 eV		EQ	[167]
	1.06 ± 0.25		PI/TES	This work
	0.9 ± 0.2 eV		EI	[168]
	0.9 ± 0.05 eV		PI	[153]
$Ar–CO^+$	1.00 ± 0.15		PI/TES	This work
		0.94	CCSD	This work
		0.93	MP4	[193]
		0.73 (D_e)	VB	[172]
	0.70 ± 0.06		PI	[192]
		0.68	VB	[194]
$Ar–N_2^+$	1.19 ± 0.10		PI/TES	This work
	1.16 eV		EQ	[197]
	1.14 ± 0.1 eV		EQ	[166]
	1.05 ± 0.07 eV		CID	[170]
		1.04 (D_e)	VB	[172]
	0.98 ± 0.20		HPMS	[148]
	0.91		SIFT	[157]

Explanation of acronyms: CID: collision-induced dissociation; Diss. EI: dissociative electron impact; EI: electron impact; EQ: equilibrium measurements; HPMS: high pressure mass spectrometry; PD/TES: photodissociation/translational energy spectroscopy; PI/TES: photoionization/translational energy spectroscopy; PI: photoionization; PFI: pulsed field ionization; SIFT: selected ion flow tube; CCSD: coupled cluster with single and double excitation; Morse: Morse potential; MP2/MP4: Möller–Plesset, second and fourth order; MRCI: multireference configuration interaction; QCISD: quadratic configuration interaction with single and double excitation; VB: valence bond. For further information, see the text.

point is that the $C_2O_2^+$ ion is in fact not a cluster ion, but rather a conventional molecular ion with a C–C bond similar to that in many stable organic compounds. The photoionization induces a chemical reaction in argon/carbon monoxide clusters leading to a molecular ion, the ethylenedione ion. The neutral analog of this ion would be the elusive carbon suboxide, C_2O_2, which is now believed to be intrinsically unstable [147]. In contrast to this the binding situation in the other systems covered in this work

(Ar_3^+, $(N_2)_2^+$, $ArCO^+$, and ArN_2^+) may be regarded as weak chemical bonds with finite electron delocalization. The binding energies of the latter are all on the order of 1–1.2 eV, stronger than expected for a pure ion/induced dipole interaction.

We finally point out that all of the cluster ions discussed in this work have a well defined equilibrium geometry. For some of the neutral precursors this does not seem to be the case, e.g., the potential curve of the $(CO)_2$, is extremely flat, exhibiting several energy minima within about 12 meV. The usage of the term 'structure' with these extremely floppy cluster systems is disputable.

6. Outlook

The investigation of the KE released in the dissociative ionization of clusters has proven to be a valuable tool in determining adiabatic ionization energies. This is particularly true for systems with large geometry difference between neutral and ionic clusters. It was pointed out that one could alternatively study the vibrational or rotational state distribution of cluster fragments. In a coincidence experiment the target density may be too small for this, but in laser-based experiments Valentini and coworkers [219] recently measured the rotational state distribution of fragments from the photolysis of HCl dimers.

At present the TES yields best results for small clusters, i.e., dimers or trimers. Application to larger clusters would lead to two problems. The first is arising from the inherent presence of a distribution of cluster sizes in a conventional cluster beam. Due to this distribution the assignment of the KER observed to one particular parent cluster may become ambiguous for broad size distributions. Here, it would be very interesting to perform TES experiments on neutral clusters with well defined size. Buck has introduced an elegant way to form size-selected cluster beams [220] by scattering from a helium beam. In yet another approach neutral size-selected clusters may also be formed by photodetachment from the corresponding cluster anion [221]. The latter technique might be limited to strongly bound neutral clusters, since dissociative electron detachment may possibly dominate in the case of van der Waals clusters. Even if a size-selected cluster beam is available, the second problem is that the fraction of the excess energy going into KER decreases with the number of internal degrees of freedom of the fragment ion, i.e., with the size of the cluster. Thus, the sensitivity of the TES technique decreases with the size of the cluster.

For small systems with few vibrational degrees of freedom a very powerful technique is to measure the PFI-PES with vibrational or even rotational resolution. For the argon dimer Signorell and Merkt [108] and Onuma et al. [127] have derived accurate spectroscopic parameters and potential curves and consequently the adiabatic IE from such an approach. However, the PFI spectroscopy is subject to the same limitation as all other direct ionization techniques, i.e., the poor Franck–Condon factors at the adiabatic IE. In the argon dimer work this is reflected in the fact that the first three ionic vibrational states ($v = 0$–2) are not observed. The entire analysis is based on the assignment that the first state observed is $v = 3$. While this conclusion is to the best of our knowledge correct in the case of the argon dimer, poor Franck–Condon factors may introduce considerable uncertainty in other systems. We note, that the observed term energies of [108,127] could also be fitted by assuming an IE just shifted up or down by one vibrational quantum with a mean absolute deviation of less than 1 cm^{-1}. Here the TES provides valuable additional support for the IE derived from the PFI experiments since it neither depends on spectroscopic assignment nor is it restricted by poor Franck–Condon factors. Similar to the TES technique the PFI-PES is also expected to yield the best results for small clusters, at least for the systems discussed in this review. For larger clusters the assignment of an electron signal to a particular parent cluster will become difficult. Furthermore it may difficult to obtain vibrationally resolved electronic spectra of the cluster ions due to the additional degrees of freedom.

For the future it seems rewarding to further test statistical theories of cluster dissociation as has recently been discussed by Parneixa and Brechignac

[222]. Such studies are expected to provide valuable insight into the energy balance of cluster fragmentation, in particular the conservation of angular momentum. The KER analysis presented in the current review suggested that often cluster fragments will be formed with a significant amount of rotational energy. It some cases even bimodal rotational state distributions might occur. It seems rewarding to test this hypothesis by looking at ion/molecule reactions of cluster ions formed from dissociative ionization. In the case of molecular ions similar studies have shown to be viable [223].

Acknowledgements

Financial support of this work by the Deutsche Forschungsgemeinschaft is gratefully acknowledged. We also thank H. Baumgärtel for his encouragement during this project.

Appendix A

In this Appendix A the molecular parameters used in the phase space calculations of the KER in the dissociative formation of Ar_2^+, $ArCO^+$ and ArN_2^+ ion are listed.

A.1. Formation of Ar_2^+

A.1.1. Reactant ion Ar_3^+

Rotational constant of the two-dimensional rotor: $B = 0.921\,\text{GHz}$, translational/rotational temperature: 27 K, vibrational temperature: 40 K.

A.1.2. Product ion Ar_2^+

Rotational constant of the two-dimensional rotor: $B = 4.107\,\text{GHz}$, vibrational frequency: $293\,\text{cm}^{-1}$.

A.2. Formation of $ArCO^+$

A.2.1. Reactant ion Ar_2CO^+

Rotational constants: $B = 4.886, 1.825, 1.329\,\text{GHz}$. The average rotational constant B is calculated from $B = (B_1 B_2 B_3)^{0.5} = 2.280\,\text{GHz}$, translational/rotational temperature: 40 K, vibrational temperature: 60 K.

A.2.2. Product ion $ArCO^+$

Rotational constants: $B = 385.5, 3.722, 3.686\,\text{GHz}$, average rotational constant $B_{\text{av}} = 17.42\,\text{GHz}$, vibrational frequencies: 100, 376, $2276\,\text{cm}^{-1}$.

A.3. Formation of ArN_2^+

A.3.1. Reactant ion $Ar_2N_2^+$

Rotational constant of the two-dimensional rotor: $B = 1.21\,\text{GHz}$, translational/rotational temperature: 40 K, vibrational temperature: 60 K.

A.3.2. Product ion ArN_2^+

Rotational constant of the two-dimensional rotor: $B = 3.665\,\text{GHz}$, vibrational frequencies: 179, 179, 311, $2344\,\text{cm}^{-1}$.

In all reactions the second product is a neutral argon atom with a polarizability of $1.64\,\text{Å}^3$ [224].

References

[1] J. Jortner, Ber. Bunsenges. Phys. Chem. 88 (1984) 188.
[2] K. Jucks, R.E. Miller, J. Chem. Phys. 88 (1988) 2196.
[3] K. Jucks, R.E. Miller, J. Chem. Phys. 88 (1988) 6059.
[4] K.-M. Weitzel, J. Booze, T. Baer, Z. Phys. D 18 (1991) 383.
[5] B. Brutschy, J. Phys. Chem. 94 (1990) 8637.
[6] I. Prigione, S.A. Rice (Eds.), Evolution of Size Effects in Chemical Dynamics, Part 1 + 2, Adv. Chem. Phys. 70 (1988).
[7] R.G. Keesee, A.W. Castleman Jr., J. Phys. Chem. Ref. Data 15 (1986) 1011.
[8] C.Y. Ng, T. Baer, I. Powis (Eds.), Cluster Ions, Wiley, Chichester, 1993.
[9] J.P. Maier (Ed.), Ion and Cluster Ion Spectroscopy and Structure, Elsevier, Amsterdam, 1989.
[10] P. Kebarle, Ann. Rev. Phys. Chem. 28 (1977) 445.
[11] W. Lindinger, in: J.H. Futrell (Ed.), Gaseous Ion Chemistry and Mass Spectrometry, Wiley, New York, 1986.
[12] J. Troe, in: C.Y. Ng, M. Baer (Eds.), State-Selected and State-to-State Ion/Molecule Reaction Dynamics, Part 2, Adv. Chem. Phys. 82 (1992) 485.
[13] E.J. Bieske, O. Dopfer, Chem. Rev. 100 (2000) 3963.
[14] C.Y. Ng, in: C.Y. Ng (Ed.), Vacuum Ultraviolet Photoionization and Photodissociation of Molecules and Clusters, World Scientific, Singapore, 1991.

[15] R.G. Cooks, J.H. Beynon, R.M. Caprioli, G.R. Lester, Metastable Ions, Elsevier, Amsterdam, 1973.
[16] T. Baer, in: M.T. Bowers (Ed.), Gas Phase Ion Chemistry, Vol. 1, Academic Press, New York, 1979.
[17] T. Baer, J. Booze, K.-M. Weitzel, in: C.Y. Ng (Ed.), Vacuum Ultraviolet Ionization and Dissociation of Molecules and Clusters, World Scientific, Singapore, 1991.
[18] J.H.D. Eland, Int. J. Mass Spectrom. Ion Phys. 9 (1972) 397.
[19] F. Güthe, K.-M. Weitzel, Chem. Phys. Lett. 251 (1996) 295.
[20] C.Y. Ng, Adv. Chem. Phys. 52 (1983) 263.
[21] T.D. Märk, A.W. Castleman Jr., Adv. At. Mol. Phys. 20 (1985) 65.
[22] T.D. Märk, Int. J. Mass Spectrom. Ion Proc. 79 (1987) 1.
[23] C.E. Klots, J. Chem. Phys. 83 (1985) 5854.
[24] E.E. Ferguson, C.R. Albertoni, R. Kuhn, Z.Y. Chen, R.G. Keesee, A.W. Castleman Jr., J. Chem. Phys. 88 (1988) 6335.
[25] E. Buonomo, F.A. Gianturco, Mol. Eng. 7 (1997) 185.
[26] T.R. Horn, R.B. Gerber, J.J. Valentini, M.A. Ratner, J. Chem. Phys. 94 (1991) 6728.
[27] H.-U. Böhmer, S.D. Peyerimhoff, Z. Phys. D 4 (1986) 195.
[28] T. Baer, Adv. Chem. Phys. 64 (1986) 111.
[29] E. Holub-Krappe, G. Ganteför, G. Bröker, A. Ding, Z. Phys. D 10 (1988) 319.
[30] J.A. Booze, T. Baer, J. Chem. Phys. 96 (1992) 5541.
[31] J.S. Riley, T. Baer, Int. J. Mass Spectrom. Ion Proc. 131 (1994) 295.
[32] K. Furuya, K. Kimura, J. Chem. Phys. 97 (1992) 1022.
[33] C. Lifshitz, in: C.Y. Ng., T. Baer, I. Powis (Eds.), Cluster Ions, Wiley, Chichester, 1993, p. 165.
[34] S. Wei, W.B. Tzeng, A.W. Castleman Jr., J. Chem. Phys. 93 (1990) 2506.
[35] J.W. Hepburn, R.J. Buss, L.J. Butler, Y.T. Lee, J. Phys. Chem. 87 (1983) 3638.
[36] P. Felder, Chimia 48 (1994) 43.
[37] W. Schnieder, W. Meier, K.-H. Welge, M.N.R. Ashfold, C.M. Western, J. Chem. Phys. 92 (1990) 7027.
[38] D.H. Mordaunt, I.R. Lambert, G.P. Morley, M.N.R. Ashfold, R.N. Dixon, L. Schnieder, K.-H. Welge, J. Chem. Phys. 98 (1993) 2054.
[39] M.A. Hanratty, J.L. Beauchamp, A.J. Illies, P.V. Köppen, M.T. Bowers, J. Am. Chem. Soc. 110 (1988) 1.
[40] R. Stockbauer, Int. J. Mass Spectrom. Ion Phys. 25 (1977) 89.
[41] H.E. Stanton, J.E. Monahan, J. Chem. Phys. 41 (1964) 3694.
[42] J.L. Franklin, P.M. Hierl, D.A. Whan, J. Chem. Phys. 47 (1967) 3148.
[43] J. Mähnert, Dissertation, Freie Universität, Berlin, 1994.
[44] K.-M. Weitzel, F. Güthe, J. Mähnert, R. Locht, H. Baumgärtel, Chem. Phys. 201 (1995) 287.
[45] F. Güthe, R. Locht, B. Leyh, H. Baumgärtel, K.-M. Weitzel, J. Phys. Chem. A 103 (1999) 8404.
[46] M.A. Haney, J.L. Franklin, J. Chem. Phys. 48 (1968) 4093.
[47] C.E. Klots, J. Chem. Phys. 58 (1973) 5364.
[48] C.E. Klots, Z. Naturforsch. 27a (1972) 553.
[49] W. Forst, Theory of Unimolecular Reactions, Academic Press, New York, 1973.
[50] W.J. Chesnavich, L. Bass, T. Su, M.T. Bowers, J. Chem. Phys. 74 (1981) 2228.
[51] M.T. Bowers, in: M.T. Bowers (Ed.), Gas Phase Ion Chemistry, Academic Press, New York, 1979.
[52] J. Mähnert, H. Baumgärtel, K.-M. Weitzel, J. Chem. Phys. 107 (1997) 6667.
[53] M.J. Frisch, M. Head-Gordon, G.W. Trucks, J.B. Foresman, H.B. Schlegel, K. Raghavachari, M.A. Robb, J.S. Binkley, C. Gonzalez, D.J. DeFrees, D.J. Fox, R.A. Whiteside, R. Seeger, C.F. Melius, J. Baker, R.L. Martin, L.R. Kahn, J.J.P. Stewart, S. Topiol, J.A. Pople, Gaussian'90, Gaussian Inc., Pittsburgh, PA, 1990.
[54] M.J. Frisch, G.W. Trucks, H.B. Schlegel, G.E. Scuseria, M.A. Robb, J.R. Cheeseman, V.G. Zakrzewski, J.A. Montgomery Jr., R.E. Stratmann, J.C. Burant, S. Dapprich, J.M. Millam, A.D. Daniels, K.N. Kudin, M.C. Strain, O. Farkas, J. Tomasi, V. Barone, M. Cossi, R. Cammi, B. Mennucci, C. Pomelli, C. Adamo, S. Clifford, J. Ochterski, G.A. Petersson, P.Y. Ayala, Q. Cui, K. Morokuma, D.K. Malick, A.D. Rabuck, K. Raghavachari, J.B. Foresman, J. Cioslowski, J.V. Ortiz, A.G. Baboul, B.B. Stefanov, G. Liu, A. Liashenko, P. Piskorz, I. Komaromi, R. Gomperts, R.L. Martin, D.J. Fox, T. Keith, M.A. Al-Laham, C.Y. Peng, A. Nanayakkara, C. Gonzalez, M. Challacombe, P.M.W. Gill, B. Johnson, W. Chen, M.W. Wong, J.L. Andres, C. Gonzalez, M. Head-Gordon, E.S. Replogle, J.A. Pople, Gaussian'98, Gaussian Inc., Pittsburgh, PA, 1998.
[55] J.A. Pople, R.K. Nesbet, J. Chem. Phys. 22 (1959) 571.
[56] C. Möller, M.S. Plesset, Phys. Rev. 46 (1934) 618.
[57] J.A. Pople, M. Head-Gordon, K. Raghavachari, J. Chem. Phys. 87 (1987) 5968.
[58] R.S. Mulliken, J. Chem. Phys. 23 (1955) 1833.
[59] J.E. Carpenter, F. Weinhold, J. Mol. Struct. (Theochem.) 169 (1988) 41.
[60] D.E. Woon, T.H. Dunning Jr., J. Chem. Phys. 98 (1993) 1358.
[61] W.J. Hehre, L. Radom, P.V.R. Schleyer, J.A. Pople, Ab Initio Molecular Orbital Theory, Wiley, New York, 1986.
[62] J.E. Del Bene, D.H. Aue, I. Shavitt, J. Am. Chem. Soc. 114 (1992) 1631.
[63] K.-M. Weitzel, J. Mähnert, H. Baumgärtel, Ber. Bunsenges. Phys. Chem. 97 (1993) 134.
[64] K.-M. Weitzel, J. Mähnert, Z. Phys. Chem. 195 (1996) 181.
[65] K.-M. Weitzel, Unimolekulare Elementarreaktionen in Molekül- und Cluster-Ionen, Shaker-Verlag, Aachen, 1998.
[66] T. Baer, W. Peatman, E.W. Schlag, Chem. Phys. Lett. 4 (1969) 243.
[67] R. Spohr, P.M. Guyon, W.A. Chupka, J. Berkowitz, Rev. Sci. Instrum. 42 (1971) 1872.
[68] T. Hsieh, J. Gilman, M. Meiss, G.G. Meisels, P.M. Hierl, Int. J. Mass Spectrom. Ion Proc. 36 (1980) 317.
[69] S.G. Lias, J.E. Bartmess, J.F. Liebman, J.L. Holmes, R.D. Levin, W.G. Mallard, J. Phys. Chem. Ref. Data 17 (Suppl. 1) (1988).
[70] K. Kimura, S. Katsumata, Y. Achiba, T. Yamazaki, S. Iwata, Handbook of HeI Photoelectron Spectra of Fundamental Organic Molecules, Japan Scientific Society Press, Tokyo, 1981.

[71] D. Klar, K. Harth, J. Ganz, T. Kraft, M.-W. Ruf, H. Hotop, V. Tsemekhman, K. Tsemekhman, M.Y. Amusia, Z. Phys. D 23 (1992) 101.
[72] G.C. King, M. Zubek, P.M. Rutter, H.H. Read, J. Phys. E: Sci. Instrum. 20 (1987) 440.
[73] Y.L. Morioka, T. Matsui, T. Tanaka, H. Yoshii, R.I. Hall, T. Hayaishi, K. Ito, J. Chem. Phys. 102 (1995) 1553.
[74] G. Reiser, W. Habenicht, K. Müller-Dethlefs, E.W. Schlag, Chem. Phys. Lett. 152 (1988) 119.
[75] K.-M. Weitzel, M. Malow, G.K. Jarvis, T. Baer, Y. Song, C.Y. Ng, J. Chem. Phys. 111 (1999) 8267.
[76] G.K. Jarvis, K.-M. Weitzel, M. Malow, T. Baer, Y. Song, C.Y. Ng, Rev. Sci. Instrum. 70 (1999) 3892.
[77] E.W. Schlag (Ed.), Time-of-flight Mass Spectrometry and its Applications, Int. J. Mass Spectrom. Ion Proc. 131 (1994) (special issue).
[78] W.C. Wiley, I.H. McLaren, Rev. Sci. Instrum. 26 (1955) 1150.
[79] G. Scoles (Ed.), Atomic and Molecular Beam Methods, Oxford University Press, New York, 1989.
[80] P. Wegener (Ed.), Molecular Beams and Low Density Gas Dynamics, Marcel Dekker, New York, 1974.
[81] D.H. Levy, Ann. Rev. Phys. Chem. 31 (1980) 197.
[82] R.E. Smalley, L. Wharton, D.H. Levy, Acc. Chem. Res. 10 (1977) 139.
[83] K.-M. Weitzel, J. Booze, T. Baer, Chem. Phys. 150 (1991) 263.
[84] J. Anderson, J. Fenn, Phys. Fluids 8 (1965) 780.
[85] H. Haberland (Ed.), Clusters of Atoms and Molecules, Springer Series in Chemical Physics (No. 52 and 56), Vol. I + II, Springer, Berlin, 1994.
[86] M. Kappes, S. Leutwyler, in: G. Scoles (Ed.), Atomic and Molecular Beam Methods, Oxford University Press, New York, 1989.
[87] E.W. Becker, Z. Phys. D 3 (1986) 101.
[88] O.F. Hagena, W. Obert, J. Chem. Phys. 56 (1972) 1793.
[89] J. Wörmer, V. Guzielski, J. Stapelfeldt, G. Zimmerer, T. Möller, Phys. Scripta 41 (1990) 490.
[90] C. Kunz (Ed.), Synchrotron Radiation, Topics in Current Physics, Vol. 10, Springer, Berlin, 1979.
[91] K. Wille, Physik der Teilchenbeschleuniger und Synchrotronstrahlungs-quellen, Teubner, Stuttgart, 1992.
[92] G. Margaritondo, Introduction to Synchrotron Radiation, Oxford University Press, Oxford, 1988.
[93] Research at BESSY, A Users Handbook, BESSY GmbH, Berlin, 1993.
[94] J.A.R. Samson, Techniques of Vacuum Ultraviolet Spectroscopy, Wiley, New York, 1967.
[95] I. Last, T.F. George, in: C.Y. Ng, T. Baer, I. Powis (Eds.), Cluster Ions, Wiley, Chichester, 1993, p. 319.
[96] J. Parson, P. Siska, Y.T. Lee, J. Chem. Phys. 56 (1972) 1511.
[97] D.E. Woon, Chem. Phys. Lett. 204 (1993) 29.
[98] Y. Tanaka, K. Yoshino, J. Chem. Phys. 53 (1970) 2012.
[99] R.O. Watts, I.J. McGee, Liquid States Chemical Physics, Wiley, New York, 1976.
[100] R.J. Le Roy, J. Chem. Phys. 57 (1972) 573.
[101] R. Aziz, M. Slaman, Mol. Phys. 58 (1986) 679.
[102] T. Gonzalez-Lezana, J. Rubayo-Soneira, S. Miret-Artes, F.A. Gianturco, G. Delgado-Barrio, P. Villarreal, J. Chem. Phys. 110 (1999) 9000.
[103] P.J. Kuntz, J. Hogreve, J. Chem. Phys. 95 (1991) 156.
[104] S.W. Rick, D.L. Lynch, J.D. Doll, J. Chem. Phys. 95 (1991) 3506.
[105] H.-U. Böhmer, S.D. Peyerimhoff, Z. Phys. D 11 (1989) 239.
[106] E.C.M. Chen, J.G. Dojahn, W.E. Wentworth, J. Phys. Chem. A 101 (1997) 3088.
[107] F.X. Gadea, I. Paidarova, Chem. Phys. 209 (1996) 281.
[108] R. Signorell, F. Merkt, J. Chem. Phys. 109 (1998) 9762.
[109] P.M. Dehmer, J.L. Dehmer, J. Chem. Phys. 69 (1978) 125.
[110] Y. Morioka, M. Ogawa, T. Matsumoto, K. Ito, K. Tanaka, T. Hayaishi, J. Phys. B 24 (1990) 791.
[111] Y. Morioka, H. Masuda, Y. Lu, K. Tanaka, T. Hayaishi, J. Phys. B 25 (1992) 5343.
[112] W.R. Wadt, J. Chem. Phys. 68 (1978) 402.
[113] H.H. Michels, R.H. Hobbs, L.A. Wright, J. Chem. Phys. 69 (1978) 5151.
[114] H.H. Michels, R.H. Hobbs, L.A. Wright, Appl. Phys. Lett. 35 (1979) 153.
[115] M.T. Bowers, W. Palke, K. Robins, C. Roehl, S. Walsh, Chem. Phys. Lett. 180 (1991) 235.
[116] F.X. Gadea, M. Amarouch, Chem. Phys. 140 (1990) 385.
[117] T. Ikegami, T. Kondow, S. Iwata, J. Chem. Phys. 98 (1993) 3038.
[118] Z.Y. Chen, B.D. May, A.W. Castleman Jr., Z. Phys. D 25 (1993) 239.
[119] W.R. Wadt, Appl. Phys. Lett. 38 (1981) 1030.
[120] F. Ragnetti, C. Zuhrt, L. Zuelicke, in: M. Chergui (Ed.), Femtochemistry Ultrafast Chem. Phys. Processes Mol. Syst. (Lausanne Conference), World Scientific, Singapore, 1996, p. 272.
[121] J.T. Moseley, R.P. Saxon, B.A. Huber, P.C. Cosby, R. Abouaf, M. Tadjedine, J. Chem. Phys. 67 (1977) 1659.
[122] R.I. Hall, Y. Lu, Y. Morioka, T. Matsui, T. Tanaka, H. Yoshii, T. Hayaishi, K. Ito, J. Phys. B: At. Mol. Opt. Phys. 28 (1995) 2435.
[123] P.M. Dehmer, S.T. Pratt, J. Chem. Phys. 76 (1982) 843.
[124] K. Norwood, J.H. Guo, C.Y. Ng, J. Chem. Phys. 90 (1989) 2995.
[125] G. Ganteför, G. Bröker, E. Holub-Krappe, A. Ding, J. Chem. Phys. 91 (1989) 7972.
[126] W. Kamke, J. de Vries, J. Krauss, E. Kaiser, B. Kamke, I.V. Hertel, Z. Phys. D 14 (1989) 339.
[127] T. Onuma, H. Yoshii, H. Ishijima, Y. Itou, T. Hayaishi, Y. Morioka, J. Mol. Spectrosc. 198 (1999) 209.
[128] J. Krauss, J. de Vries, H. Steger, E. Kaiser, B. Kamke, W. Kamke, Z. Phys. D 20 (1991) 29.
[129] P. Dehmer, J. Chem. Phys. 76 (1982) 1263.
[130] Y.H. Chiu, S. Pullins, D.J. Levandier, R.A. Dressler, J. Chem. Phys. 112 (2000) 10880.
[131] C.A. Woodward, J.E. Upham, A.J. Stace, J.N. Murell, J. Chem. Phys. 91 (1989) 7612.
[132] N.G. Gotts, R. Hallett, J.A. Smith, A.J. Stace, Chem. Phys. Lett. 181 (1991) 491.

[133] H. Haberland, A. Hofmann, B.V. Issendorf, J. Chem. Phys. 103 (1995) 3450.
[134] D.A. Kirkwood, C.A. Woodward, A. Mouhandes, A.J. Stace, A. Bastida, J. Zuniga, A. Requena, F.X. Gadea, J. Chem. Phys. 113 (2000) 2175.
[135] K.-M. Weitzel, M. Penno, J. Mähnert, H. Baumgärtel, Z. Phys. D 29 (1994) 195.
[136] A. Bastida, N. Halberstadt, J.A. Beswick, F.X. Gadea, U. Buck, R. Galonska, C. Lauenstein, Chem. Phys. Lett. 249 (1996) 1.
[137] U. Buck, H. Meyer, J. Chem. Phys. 84 (1986) 4854.
[138] K. Stephan, T.D. Märk, Chem. Phys. Lett. 90 (1982) 51.
[139] P.A. Vanden Bout, J.M. Steed, L.S. Bernstein, W. Klemperer, Astrophys. J. 234 (1979) 503.
[140] M. Havenith, M. Petri, C. Lubina, G. Hilpert, W. Urban, J. Mol. Spectrosc. 167 (1994) 248.
[141] A. van der Pol, A. van der Avoird, P.E.S. Wormer, J. Chem. Phys. 92 (1990) 7498.
[142] P.R. Bunker, P. Jensen, S.C. Althorpe, D.C. Clary, J. Mol. Spectrosc. 157 (1993) 208.
[143] G.P. Raine, H.F. Schaefer III, R.C. Haddon, J. Am. Chem. Soc. 105 (1983) 194.
[144] H. Staudinger, E. Anthes, Ber. Dtsch. Chem. Ges. 46 (1913) 1426.
[145] D. Sülzle, T. Weiske, H. Schwarz, Int. J. Mass Spectrom. Ion Proc. 125 (1993) 75.
[146] H. Chen, J.L. Holmes, Int. J. Mass Spectrom. Ion Proc. 133 (1994) 111.
[147] D. Schröder, C. Heinemann, H. Schwarz, J.N. Harvey, S. Dua, S.J. Blanksby, J.H. Bowie, Chem. Eur. J. 4 (1998) 2550.
[148] M.S.B. Munson, F.H. Field, J.L. Franklin, J. Chem. Phys. 37 (1962) 1790.
[149] M. Meot-Ner, F.H. Field, J. Chem. Phys. 61 (1974) 3742.
[150] D. Gerlich, T. Rox, Z. Phys. D 13 (1989) 259.
[151] D. Muigg, G. Denifl, A. Stamatovic, O. Echt, T.D. Märk, Chem. Phys. 239 (1998) 409.
[152] G. Senn, D. Muigg, G. Denifl, A. Stamatovic, P. Scheier, T.D. Märk, Eur. Phys. J. D 9 (1999) 159.
[153] S.H. Linn, Y. Ono, C.Y. Ng, J. Chem. Phys. 74 (1981) 3342.
[154] A. Ding, J.H. Futrell, R.A. Cassidy, L. Cordis, J. Hesslich, Surf. Sci. 156 (1984) 282.
[155] K. Norwood, J.-H. Guo, G. Luo, C.Y. Ng, J. Chem. Phys. 88 (1988) 4098.
[156] K. Norwood, J.-H. Guo, G. Luo, C.Y. Ng, J. Chem. Phys. 90 (1989) 6026.
[157] J. Glosik, V. Skalsky, C. Praxmarer, D. Smith, W. Freysinger, W. Lindinger, J. Chem. Phys. 101 (1994) 3792.
[158] N.G.F. Beebe, J.R. Sabin, Chem. Phys. Lett. 24 (1974) 389.
[159] L.B. Knight Jr., J. Steadman, P.K. Miller, D.E. Bowman, E.R. Davidson, D. Feller, J. Chem. Phys. 80 (1984) 4593.
[160] J.T. Blair, J.C. Weisshaar, J.E. Carpenter, F. Weinhold, J. Chem. Phys. 87 (1987) 392.
[161] W.E. Thompson, M.E. Jacox, J. Chem. Phys. 95 (1991) 735.
[162] J. Mähnert, H. Baumgärtel, K.-M. Weitzel, J. Chem. Phys. 103 (1995) 7016.
[163] G. Herzberg, Spectra of Diatomic Molecules, 2nd Edition, Van Nostrand Reinhold, New York, 1950.
[164] B. Kukawska-Tarnawska, G. Chalasinski, K. Olszewski, J. Chem. Phys. 101 (1994) 4964.
[165] J.D. Payzant, P. Kebarle, J. Chem. Phys. 53 (1970) 4723.
[166] H.H. Teng, D.C. Conway, J. Chem. Phys. 59 (1973) 2316.
[167] K. Hiraoka, G. Nakajima, J. Chem. Phys. 88 (1988) 7709.
[168] K. Stephan, T.D. Märk, J.H. Futrell, H. Helm, J. Chem. Phys. 80 (1984) 3185.
[169] K. Norwood, G. Luo, C.Y. Ng, J. Chem. Phys. 91 (1989) 849.
[170] R. Schultz, P.B. Armentrout, Int. J. Mass Spectrom. Ion Proc. 107 (1991) 29.
[171] S.C. de Castro, H.F. Schaeffer III, R.M. Pitzer, J. Chem. Phys. 74 (1981) 550.
[172] J.H. Langenberg, I.B. Bucur, P. Archirel, Chem. Phys. 221 (1997) 225.
[173] C. Leonard, P. Rosmus, S. Carter, N. Handy, J. Phys. Chem. A 103 (1999) 1846.
[174] L.B. Knight Jr., K.D. Johnessen, D.C. Cobranchi, E.A. Earl, D. Feller, E.R. Davidson, J. Chem. Phys. 87 (1987) 885.
[175] H. Linnartz, D. Verdes, P.J. Knowles, N.M. Lakin, P. Rosmus, J.P. Maier, J. Chem. Phys. 113 (2000) 895.
[176] G.A. Parker, R.T. Pack, J. Chem. Phys. 69 (1978) 3268.
[177] K. Mirsky, Chem. Phys. 46 (1980) 445.
[178] J. Tennyson, S. Miller, B.T. Sutcliffe, J. Chem. Soc., Faraday Trans. 2 (1988) 1295.
[179] C.A. Parish, J.D. Augspurger, C.E. Dykstra, J. Phys. Chem. 96 (1992) 2069.
[180] B. Kukawska-Tarnawska, G. Chalasinski, K. Olszewski, J. Chem. Phys. 101 (1994) 4964.
[181] G. Jansen, Chem. Phys. Lett. 223 (1994) 377.
[182] S. Shin, S.K. Shin, F.-M. Tao, J. Chem. Phys. 104 (1996) 183.
[183] R.R. Toczylowski, S.M. Cybulski, J. Chem. Phys. 112 (2000) 4604.
[184] T. Ogata, W. Jäger, I. Ozier, M.C.L. Gerry, J. Chem. Phys. 98 (1993) 9399.
[185] A.R.W. McKellar, Y.P. Zeng, S.W. Sharpe, C. Wittig, R.A. Beaudet, J. Mol. Spectrosc. 153 (1992) 475.
[186] M. Havenith, G. Hilpert, M. Petri, W. Urban, Mol. Phys. 81 (1994) 1003.
[187] M. Hepp, R. Gendriesch, I. Pak, Y.A. Kuritsyn, F. Lewen, G. Winnewisser, M. Brookes, A.R.W. McKellar, J.K.G. Watson, T. Amano, Mol. Phys. 92 (1997) 229.
[188] A.R.W. McKellar, Mol. Phys. 98 (2000) 111.
[189] I. Scheele, R. Lehnig, M. Havenith, Mol. Phys. 99 (2001) 197.
[190] I. Scheele, R. Lehnig, M. Havenith, Mol. Phys. 99 (2001) 205.
[191] V. Castells, N. Halberstadt, S.K. Shin, R.A. Beaudet, C. Wittig, J. Chem. Phys. 101 (1994) 1006.
[192] K. Norwood, J.-H. Guo, G. Luo, C.Y. Ng, Chem. Phys. 129 (1989) 109.
[193] P.A. Hamilton, A.N. Highes, K.D. Sales, J. Chem. Phys. 99 (1993) 436.
[194] P. Archirel, Chem. Phys. 193 (1995) 55.

[195] K.-M. Weitzel, Chem. Phys. 237 (1998) 43.
[196] W. Kaul, R. Fuchs, Z. Naturforsch. 15a (1960) 326.
[197] K. Hiraoka, S. Fujimaki, M. Nasu, A. Minamitsu, S. Yamabe, H. Kouno, J. Chem. Phys. 107 (1997) 2550.
[198] A.A. Viggiano, R.A. Morris, J. Chem. Phys. 99 (1993) 3527.
[199] D. Smith, N.G. Adams, Phys. Rev. A 23 (1981) 2327.
[200] W. Lindinger, F. Howorka, P. Lukc, S. Kuhn, H. Villinger, E. Alge, H. Rammler, Phys. Rev. A 23 (1981) 2319.
[201] P.M. Guyon, T.R. Grovers, T. Baer, Z. Phys. D 4 (1986) 89.
[202] M. Hawley, M.A. Smith, J. Phys. Chem. 96 (1992) 6693.
[203] S. Schlemmer, T. Kuhn, E. Lescop, D. Gerlich, Int. J. Mass. Spectrom. 185–187 (1999) 589.
[204] M.R. Spalburg, E.A. Gislason, Chem. Phys. 94 (1985) 339.
[205] G. Parlant, E.A. Gislason, Chem. Phys. 101 (1986) 227.
[206] H.-S. Kim, M.T. Bowers, J. Chem. Phys. 93 (1990) 1158.
[207] M. Tichy, N.D. Twiddy, D.P. Wareing, N.G. Adams, D. Smith, Int. J. Mass Spectrom. Ion Proc. 81 (1987) 235.
[208] T.F. Magnera, J. Michl, Chem. Phys. Lett. 192 (1992) 99.
[209] T.F. Magnera, D.E. David, J. Michl, J. Chem. Soc., Faraday Trans. 86 (1990) 2427.
[210] K. Stephan, T.D. Märk, Chem. Phys. Lett. 87 (1982) 226.
[211] A.J. Illies, M.T. Bowers, Org. Mass Spectrom. 18 (1983) 553.
[212] T. Nagata, T. Kondow, Z. Phys. D 20 (1991) 153.
[213] M.S. Bowers, K.T. Tang, J.P. Toennies, J. Chem. Phys. 88 (1988) 5465.
[214] V. Frecer, D.C. Jain, A.-M. Sapse, J. Phys. Chem. 95 (1991) 9263.
[215] K. Hiraoka, T. Mori, S. Yamabe, Chem. Phys. Lett. 189 (1992) 7.
[216] A.-M. Sapse, J. Phys. Chem. 89 (1994) 768.
[217] J. Mähnert, H. Baumgärtel, K.-M. Weitzel, J. Chem. Phys. 102 (1995) 180.
[218] J.A. Montgomery, J.W. Ochterski, G.A. Petersson, J. Chem. Phys. 101 (1994) 5900.
[219] C.A. Picconatto, H. Ni, A. Srivastava, J.J. Valentini, J. Chem. Phys. 114 (2001) 7073.
[220] U. Buck, J. Phys. Chem. 92 (1988) 1023.
[221] S. Wolf, G. Sommerer, S. Rutz, E. Schreiber, T. Leisner, L. Wöste, R.S. Berry, Phys. Rev. Lett. 74 (1995) 4177.
[222] P. Parneixa, P. Brechignac, Eur. Phys. J. 13 (2001) 43.
[223] J.H.M. Beijersbergen, W. van der Zande, P.G. Kistemaker, J. Los, J. Phys. Chem. 97 (1993) 11180.
[224] Handbook of Chemistry and Physics, CRC Press, Boca Raton, FL, 1988.